Spatial–temporal patterns in heterogeneous traffic flow with a variety of driver behavioural characteristics and vehicle parameters

2004 J. Phys. A: Math. Gen. 37 8753

(http://iopscience.iop.org/0305-4470/37/37/001)

INSTITUTE OF PHYSICS PUBLISHING JOURNAL OF PHYSICS A: MATHEMATICAL AND GENERAL

J. Phys. A: Math. Gen. **37** (2004) 8753–8788 PII: S0305-4470(04)78025-7

Spatial–temporal patterns in heterogeneous traffic flow with a variety of driver behavioural characteristics and vehicle parameters

Boris S Kerner[1] **and Sergey L Klenov**[2]

[1] DaimlerChrysler AG, RIC/TS, HPC: T729, 70546 Stuttgart, Germany
[2] Department of Physics, Moscow Institute of Physics and Technology, 141700 Dolgoprudny, Moscow Region, Russia

Received 17 March 2004, in final form 7 July 2004
Published 1 September 2004
Online at stacks.iop.org/JPhysA/37/8753
doi:10.1088/0305-4470/37/37/001

Abstract

A microscopic theory of spatial–temporal congested traffic patterns in heterogeneous traffic flow with a variety of driver behavioural characteristics and vehicle parameters is presented. A microscopic model for heterogeneous traffic flow is developed based on three-phase traffic theory. Diverse congested pattern features at a freeway bottleneck due to an on-ramp in heterogeneous traffic flow on a two-lane freeway are found. A numerical study of these specific pattern features and their comparison with empirical results are performed. A comparison of congested patterns in heterogeneous traffic flow with congested patterns in traffic flow with identical vehicles is made.

PACS numbers: 89.40.+k, 47.54.+r, 64.60.Cn, 64.60.Lx

1. Introduction

Traffic flow theory has been one of the most quickly developing fields of nonlinear and statistical physics during the last few years [1–13]. However, it is only recently that a 'puzzle' of spatiotemporal features of congested traffic patterns has been solved and these pattern features adequately understood [14–16, 18–21]. Consequently, earlier traffic flow theories and models [1–6] cannot explain and predict many of these empirical spatiotemporal traffic pattern features (see for more detail [16]).

To explain congested pattern features, Kerner introduced a three-phase traffic theory [14, 17]. In this theory, there are two qualitative different traffic phases that should be distinguished in congested traffic: the 'synchronized flow' and 'wide moving jam' phases. To distinguish between these traffic phases in congested traffic, some objective (empirical) criteria should be applied [18–20] (see also [15]). The downstream front of a wide moving jam propagates on a freeway while *maintaining* the mean velocity of this front even if the wide

moving jam propagates through any complex traffic state and through freeway bottlenecks. In contrast, the downstream front of the 'synchronized flow' phase (where vehicles accelerate from synchronized flow to free flow) is usually fixed at the bottleneck. As a proof of the three-phase traffic theory its results can be considered (see [22–24] and this paper), which enable us to overcome the mentioned problems of earlier models for description of congested traffic. The results of [22, 23] have recently been confirmed by studies of other microscopic models in the context of the three-phase traffic theory [25–27].

There are also models and theories where congested traffic pattern features should be explained and predicted based on either different driver behavioural characteristics (e.g., [28, 29]) or different vehicle parameters (e.g., [30]). In these theories, differences in driver behavioural characteristics [28, 29] or in vehicle parameters [30] should be responsible for the onset of congestion and other fundamental empirical features of congested patterns. However, this approach is also in contradiction with empirical observations.

To explain this, let us note that there are empirical features of phase transitions and spatial–temporal congested patterns at freeway bottlenecks that are reproducible in traffic observations over many days and years on freeways in various countries. Thus, these qualitative empirical features remain in traffic flows with very different driver behavioural characteristics and vehicle parameters. Examples of these *fundamental* empirical features of the phase transitions and congested patterns at freeway bottlenecks are (i) the probabilistic nature of speed breakdown and freeway capacity at a bottleneck (e.g., [31, 32]; see references in [33–35]); (ii) speed breakdown at a bottleneck is associated with a phase transition from free to synchronized flow (F$\rightarrow$S transition) rather than with wide moving jam emergence [14, 15]; (iii) wide moving jams can emerge spontaneously only in synchronized flow [14]. These and other fundamental features of the phase transitions and of spatial–temporal traffic patterns are considered in more detail in the book [36].

Neither the probabilistic feature of the breakdown phenomenon nor spontaneous moving jam emergence can be shown mathematically and predicted in the behavioural theory [28, 29] where differences in driver behavioural characteristics should be responsible for empirical features of congested traffic. The model with different vehicle characteristics [30] shows qualitatively the same traffic features at on-ramp bottlenecks as those associated with some other models reviewed in [1–6] where only one type of vehicle is considered. In particular, in [4, 30] moving jams occur spontaneously in free flow at an on-ramp bottleneck if the flow rate upstream of the on-ramp is sufficiently high and the flow rate to the on-ramp gradually increases from zero. This is in qualitative contradiction with empirical results of congested pattern formation [15]. Thus, an introduction of different driver characteristics and/or different vehicle parameters [28–30] in the context of freeway traffic flow models reviewed in [1–6] does not lead to an adequate theoretical description of empirical spatial–temporal congested freeway traffic patterns.

In [22–24], we have shown that microscopic traffic flow models with identical vehicles based on three-phase traffic theory can predict all mentioned and other fundamental empirical features of spatial–temporal congested patterns [15]. However, it is obvious that in real traffic there are drivers with very different characteristics and vehicles that have very different parameters (e.g., different desired and different safe driver speeds, aggressive and timid driver behaviour, vehicles and long vehicles, and so on). Therefore, we can expect that differences in driver behavioural characteristics and vehicle parameters should be of some influence on characteristics of spatial–temporal congested patterns found in the microscopic three-phase traffic theory with identical vehicles [22–24]. In this paper, a microscopic three-phase traffic theory of spatial–temporal congested patterns in heterogeneous traffic flow with different driver behavioural characteristics and vehicle parameters is developed.

The paper is organized as follows. In section 2, the model of [24] is further developed for heterogeneous traffic flow with different driver behavioural characteristics and vehicle parameters. Congested pattern features on a two-lane freeway in homogeneous flow with identical vehicles are considered in section 3. Results of a numerical study of diverse spatial–temporal congested patterns in heterogeneous flow and their features are considered in sections 4 and 5. In section 6 some general properties of congested pattern propagation in heterogeneous flow are discussed.

2. Microscopic two-lane model for heterogeneous flow with a variety of driver behavioural characteristics and vehicle parameters

In a microscopic traffic flow model for heterogeneous flow, there are three types of vehicles: 'fast', 'slow' and 'long' vehicles. Fast and slow vehicles have the same length that is shorter than the length of long vehicles. The maximum speed in free flow of fast vehicles is higher than that for slow and long vehicles. There are also other model parameters, which are different for different drivers and vehicles. In the model, fast, slow and long vehicles are specified by a vehicle identifier j. The vehicle identifier is $j = 1$ for fast vehicles, it is $j = 2$ for slow vehicles and it is $j = 3$ for long vehicles. All model parameters and variables, which are chosen in the model different for the three types of vehicles, are marked by superscripts (j) where $j = 1, 2$ and 3. The percentages of fast $\eta^{(1)}$, slow $\eta^{(2)}$ and long vehicles $\eta^{(3)}$ in heterogeneous flow satisfy the obvious condition

$$\eta^{(1)} + \eta^{(2)} + \eta^{(3)} = 100\%. \tag{1}$$

2.1. Single-lane model

In a spatial continuum and discrete-time single-lane model, the general rules of vehicle motion from [22, 24] are used:

$$v_{n+1} = \max(0, \min(v_{\text{free}}, v_{\text{c},n}, v_{\text{s},n})), \tag{2}$$

$$x_{n+1} = x_n + v_{n+1}\tau, \tag{3}$$

$$v_{\text{c,n}} = \begin{cases} v_n + \Delta_n & \text{at } x_{\ell,n} - x_n \leqslant D_n \\ v_n + a_n\tau & \text{at } x_{\ell,n} - x_n > D_n, \end{cases} \tag{4}$$

where

$$\Delta_n = \max(-b_n\tau, \min(a_n\tau, v_{\ell,n} - v_n)). \tag{5}$$

In (2)–(5), v_n and x_n are respectively the vehicle speed and space coordinate of the vehicle (vehicle front); the index n corresponds to the discrete time $t = n\tau, n = 0, 1, 2, \ldots$; τ is the time step; v_{free} is the maximum speed in free flow; $v_{\text{s,n}}$ is the safe speed; the lower index ℓ marks variables related to the vehicle in front of that at x_n, the preceding vehicle; a_n is a vehicle acceleration; values $a_n \geqslant 0$ and $b_n \geqslant 0$ in (4), (5) are chosen to restrict changes in speed when the vehicle accelerates or adopts its speed to the speed of the preceding vehicle. The adaptation of the speed to the speed of the preceding vehicle is described by formulae (2), (4), (5) and takes place within a synchronization distance D_n: at $x_{\ell,n} - x_n \leqslant D_n$ the vehicle decelerates if $v_n > v_{\ell,n}$, and accelerates if $v_n < v_{\ell,n}$ [22]. The rules (4) [22] are some of the possible microscopic approaches to the modelling of a driver's behaviour when the driver approaches synchronized flow or the driver is within synchronized flow, i.e., these rules describe human expectation of the related local driving conditions. At sufficiently large

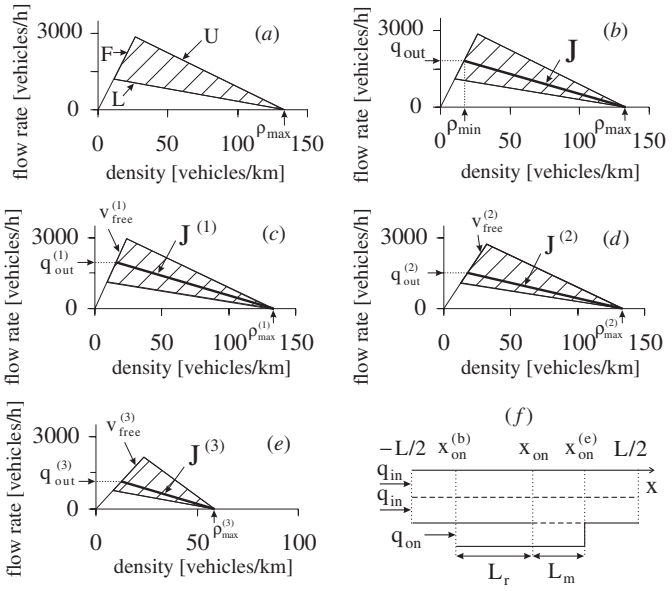

Figure 1. (*a*) Steady states in the flow–density plane. (*b*)–(*e*) Steady states together with lines J in the model of traffic flow with identical vehicles (*b*) (see sections 2.5.3 and 3) and the models of traffic flow for the limiting cases in which all vehicles are fast (*c*), slow (*d*) and long vehicles (*e*). (*f*) Model of an on-ramp bottleneck. In (*a*) the two-dimensional region in the flow–density plane (dashed region) is limited by three boundaries U, L and F that are related to the safe speed, the synchronization distance and the maximum free flow speed, respectively, as explained in [22, 23]. At chosen model parameters (section 2.5) the flow rate in the outflow from a wide moving jam and the velocity of the downstream jam front are $q_{\rm out} = 1810\,{\rm vehicles\,h^{-1}}$ and $v_{\rm g} = -15.5$ km h^{-1} for the model of identical vehicles, $q_{\rm out}^{(1)} =$ 1900 vehicles h^{-1} and $v_{\rm g}^{(1)} = -16.2$ km h^{-1} for fast vehicles, $q_{\rm out}^{(2)} = 1510$ vehicles h^{-1} and $v_{\rm g}^{(2)} = -13$ km h^{-1} for slow vehicles, $q_{\rm out}^{(3)} = 1130$ vehicles h^{-1} and $v_{\rm g}^{(3)} = -24.5$ km h^{-1} for long vehicles, respectively.

distances from the preceding vehicle, the vehicle simply accelerates. However, if the driver cannot pass the preceding vehicle, then within the synchronization distance the vehicle tends to adjust its speed to the preceding vehicle, i.e., it decelerates if it is faster, and accelerates if it is slower than the preceding vehicle.

The synchronization distance as shown in [22, 23] is related to the fundamental hypothesis of three-phase traffic theory [14]: hypothetical steady states of synchronized flow cover a 2D region in the flow–density plane (figures 1(*a*), (*b*)).

In the general rules of vehicle motion (2)–(5), the synchronization distance D_n depends on the vehicle speed v_n and on the speed of the preceding vehicle $v_{\ell,n}$

$$D_n = d_\ell + G(v_n, v_{\ell,n}), \tag{6}$$

where the function $G(u, w)$ is

$$G(u, w) = \max(0, k\tau u + \beta a^{-1} u(u - w)), \tag{7}$$

$k > 1$ and β are constants, a is the maximum acceleration, d_ℓ is the length of the preceding vehicle that can be different from the vehicle length d. If $v_n = v_{\ell,n}$, from (6) and (7), we get that the synchronization distance $D_n = d_\ell + k v_n \tau$. If $v_n > v_{\ell,n}$, the distance D_n increases and vice versa.

2.1.1. Motion state model for random acceleration and deceleration. As in some other traffic flow models [3, 4, 37–41], in the model, we use variables that are stochastic functions. *At the first step*, the preliminary speed of each vehicle is set to $\tilde{v}_{n+1} = v_{n+1}$ where v_{n+1} is calculated based on (2)–(6). *At the second step*, a noise component ξ_n is added to the calculated speed $\tilde{v}_{n+1}$ and then the final value of the speed v_{n+1} at time $n+1$ is found from the condition introduced in [23]

$$v_{n+1} = \max(0, \min(v_{\text{free}}, \tilde{v}_{n+1} + \xi_n, v_n + a\tau, v_{s,n})). \tag{8}$$

In the model, a random deceleration and acceleration are applied depending on whether the vehicle decelerates or accelerates or else maintains its speed:

$$\xi_n = \begin{cases} -\xi_{\text{b}} & \text{if} \quad S_{n+1} = -1 \\ \xi_{\text{a}} & \text{if} \quad S_{n+1} = 1 \\ 0 & \text{if} \quad S_{n+1} = 0, \end{cases} \tag{9}$$

where ξ_{b} and ξ_{a} are random sources for deceleration and acceleration, respectively ($\xi_{\text{b}}, \xi_{\text{a}} \geqslant 0$); S in (9) denotes the state of motion ($S_{n+1} = -1$ is related to a deceleration, $S_{n+1} = 1$ to an acceleration and $S_{n+1} = 0$ to the motion at nearly constant speed)

$$S_{n+1} = \begin{cases} -1 & \text{if} \quad \tilde{v}_{n+1} < v_n - \delta \\ 1 & \text{if} \quad \tilde{v}_{n+1} > v_n + \delta \\ 0 & \text{otherwise}, \end{cases} \tag{10}$$

where δ is a constant ($\delta \ll a\tau$).

The noise component ξ_{a} in (9) causes vehicle acceleration, which is sometimes stronger than is required; this models a vehicle 'overacceleration' [24, 36]. Accordingly, the noise component ξ_{b} in (9) models a vehicle 'overdeceleration'. ξ_{b} and ξ_{a} in (9) are chosen 'impulsive':

$$\xi_{\text{b}} = a\tau\Theta(p_{\text{b}} - r), \tag{11}$$

$$\xi_{\text{a}} = a\tau\Theta(p_{\text{a}} - r). \tag{12}$$

In (11), (12), p_{b} and p_{a} are probabilities of random deceleration and acceleration, respectively; $r = \text{rand}(0, 1)$ is an independent random value uniformly distributed between 0 and 1; $\Theta(z) = 0$ at $z < 0$ and $\Theta(z) = 1$ at $z \geqslant 0$.

2.1.2. Random time delays. To simulate a time delay either in vehicle acceleration or in vehicle deceleration [3, 4], a_n and b_n in (4), (5) are taken as the following stochastic functions,

$$a_n = a\Theta(P_0 - r_1), \tag{13}$$

$$b_n = a\Theta(P_1 - r_1), \tag{14}$$

$$P_0 = \begin{cases} p_0 & \text{if} \quad S_n \neq 1 \\ 1 & \text{if} \quad S_n = 1, \end{cases} \tag{15}$$

$$P_1 = \begin{cases} p_1 & \text{if} \quad S_n \neq -1 \\ p_2 & \text{if} \quad S_n = -1, \end{cases} \tag{16}$$

where $r_1 = \text{rand}(0, 1)$, p_1 is a constant, $p_2 = p_2(v_n)$ and $p_0 = p(v_n)$ are taken as speed functions. The function P_0 in (15) determines the probability $\psi_{\text{a}} = 1 - P_0$ of a random delay in vehicle acceleration at time step $n+1$, whereas the function P_1 (16) determines the probability $\psi_{\text{b}} = 1 - P_1$ of a random delay in vehicle deceleration at time step $n+1$.

The mean time delay $\tau_{\rm del}^{\rm (a)}$ after which the vehicle starts to accelerate is $\tau_{\rm del}^{\rm (a)}(v) = \tau/p_0(v)$ [24]. The time delay $\tau_{\rm del}^{\rm (a)}(v)$ is supposed to be a decreasing function of the vehicle speed v (section 2.5). At the downstream front of a wide moving jam vehicles accelerate from the initial speed $v = 0$ within the jam with the mean time delay $\tau_{\rm del}^{\rm (a)}(0)$ [37, 39]

$$\tau_{\rm del}^{\rm (a)} = \tau_{\rm del}^{\rm (a)}(0) = \frac{\tau}{p_0(0)}. \tag{17}$$

Accordingly, vehicles start to accelerate at the downstream front of a moving synchronized flow pattern (MSP) with the mean time delay [24]

$$\tau_{\rm del}^{\rm (a)}(v_{\rm syn}) = \frac{\tau}{p_0(v_{\rm syn})}, \tag{18}$$

where $v_{\rm syn}$ is the vehicle speed upstream of the downstream front of the MSP.

The parameter p_1 in (16) determines the mean time delay $\tau_{\rm del}^{\rm (d)} = \tau/p_1$ [24] after which a vehicle starts to decelerate to adopt its speed to a lower speed of the preceding vehicle. However, if the vehicle already decelerates at time step n, it continues to decelerate at time step $n + 1$ with probability p_2 and interrupts decelerating with probability $1 - p_2$.

2.1.3. Safe speed. The safe speed $v_{{\rm s},n}$ in (2) is chosen in the form

$$v_{{\rm s},n} = \min\bigl(v_n^{\rm (safe)}, g_n/\tau + v_\ell^{\rm (a)}\bigr), \tag{19}$$

where

$$g_n = x_{\ell,n} - x_n - d_\ell, \tag{20}$$

$$v_\ell^{\rm (a)} = \max\bigl(0, \min\bigl(v_{\ell,n}^{\rm (safe)} - a\tau, v_{\ell,n} - a\tau, g_{\ell,n}/\tau\bigr)\bigr), \tag{21}$$

$v_n^{\rm (safe)} = v^{\rm (safe)}(g_n, v_{\ell,n})$ is the safe speed in the model of Krauß *et al* [41] that belongs to the Gipps-class models [42], g_n is the space gap, $v_\ell^{\rm (a)}$ (21) is an 'anticipation' speed of the preceding vehicle at the next time step, $v_{\ell,n}^{\rm (safe)}$ and $g_{\ell,n}$ are respectively the safe speed and the space gap for the preceding vehicle.

The safe speed $v^{\rm (safe)}(g_n, v_{\ell,n})$ in (19) ensures collisionless vehicle motion if $g_n \geqslant v_{\ell,n}\tau$ [43]. In the model, in some cases, namely due to lane changing or merging of vehicles onto the main road from the on-ramp lane, the gap g_n can become less than $v_{\ell,n}\tau$ for a short time. In these critical situations, collisionless vehicle motion is due to the second term in (19). Simulations show that (19), (21) lead to collisionless vehicle motion in a wide range of parameters of the merging region (section 2.4) and at the chosen lane changing rules (section 2.2).

2.1.4. Characteristics of fast, slow and long vehicles. The following parameters in the vehicle motion rules (2)–(16), (19)–(21) are chosen different for fast ($j = 1$), slow ($j = 2$) and long ($j = 3$) vehicles. The vehicle length d that includes the minimum distance between vehicles within a wide moving jam and the maximum vehicle speed $v_{\rm free}$ are

$$d = d^{(j)}, \qquad j = 1, 2, 3, \tag{22}$$

$$v_{\rm free} = v_{\rm free}^{(j)}, \qquad j = 1, 2, 3, \tag{23}$$

where $v_{\rm free}^{(1)}$, $v_{\rm free}^{(2)}$ and $v_{\rm free}^{(3)}$ are constant values[3]. The parameter k in (7) is

$$k = k^{(j)}, \qquad j = 1, 2, 3. \tag{24}$$

Two-dimensional regions of steady-state model solutions in the flow–density plane for traffic flows in which either all vehicles are fast vehicles, or all vehicles are slow vehicles, or else all vehicles are long vehicles are shown in figures 1(*c*), (*d*), (*e*), respectively.

The probabilities $p_{\rm b}$, $p_{\rm a}$ in (11), (12) and $p_0(v)$ in (15) are

$$p_{\rm b} = p_{\rm b}^{(j)}, \qquad p_{\rm a} = p_{\rm a}^{(j)}, \qquad j = 1, 2, 3, \tag{25}$$

$$p_0(v) = p_0^{(j)}(v), \qquad j = 1, 2, 3. \tag{26}$$

The latter formula leads to the different mean time delays in vehicle acceleration

$$\tau_{\rm del}^{\rm (a)}(v) = \tau_{\rm del}^{\rm (a,j)}(v) = \frac{\tau}{p_0^{(j)}(v)}, \qquad j = 1, 2, 3 \tag{27}$$

for fast ($j = 1$), slow ($j = 2$) and long vehicles ($j = 3$). The functions $p_0^{(j)}(v)$ in (27) are chosen to satisfy the conditions $p_0^{(1)}(v) > p_0^{(2)}(v) > p_0^{(3)}(v)$ (section 2.5). Then

$$\tau_{\rm del}^{\rm (a,1)}(v) < \tau_{\rm del}^{\rm (a,2)}(v) < \tau_{\rm del}^{\rm (a,3)}(v). \tag{28}$$

Corresponding to (28), fast vehicles have a time delay shorter than the related time delays for slow and long vehicles, i.e., fast vehicles prefer a more aggressive driving.

2.2. Two-lane model

Lane changing rules of the two-lane model are based on the well-known incentive and security conditions (see Nagel *et al* [46]). These conditions should be adjusted to take into account the effect of the synchronization distance and an asymmetry of lane changing in heterogeneous traffic flow.

The following incentive conditions for lane changing from the right lane to the left lane ($R \to L$) and a return change from the left lane to the right lane ($L \to R$) have been used in the model [22]:

$$R \to L: \quad v_n^+ \geqslant v_{\ell,n} + \delta_1 \quad \text{and} \quad v_n \geqslant v_{\ell,n}, \tag{29}$$

$$L \to R: \quad v_n^+ > v_{\ell,n} + \delta_2 \quad \text{or} \quad v_n^+ > v_n + \delta_2, \tag{30}$$

where $\delta_1 \geqslant 0$, $\delta_2 \geqslant 0$ are constants. Here $\delta_1 < \delta_2$ for fast vehicles and $\delta_1 > \delta_2$ for slow and long vehicles. These conditions correspond to the fact that fast vehicles prefer to move in the left lane whereas slow and long vehicles prefer the right lane.

The security conditions by lane changing are given by inequalities

$$g_n^+ > \min\bigl(v_n\tau, G_n^+\bigr), \qquad g_n^- > \min(v_n^-\tau, G_n^-), \tag{31}$$

where

$$G_n^+ = G\bigl(v_n, v_n^+\bigr), \qquad G_n^- = G(v_n^-, v_n), \tag{32}$$

the function $G(u, w)$ is given by (7).

[3] In free flow, besides different maximum vehicle speeds very different time gaps between vehicles are observed (e.g., [44, 45]). It can be assumed that these and many other empirical statistical features of free flow are associated with various driver characteristics and vehicle parameters. However, a description of statistical features of free flow is beyond the scope of this paper.

Superscripts + and − in variables, parameters and functions are related to the preceding vehicle and the trailing vehicle in a neighbouring (target) lane, respectively. Similarly to the lane changing rules in [46], the speed v_n^+ or the speed $v_{\ell,n}$ in (29), (30) is set to ∞ if the gap g_n^+ or the gap g_n exceeds a given look-ahead distance L_a, respectively. The functions G_n^+, G_n^- in (31) facilitate the synchronization of the speed across the lanes if there is a large difference between the speeds in different lanes. If (29)–(31) are satisfied, then just as in Rickert *et al* [47], in the model the vehicle changes lane with probability p_c.

It is assumed that if the speed in the right lane is high enough, slow and long vehicles moving first in the left lane are usually forced to change to the right lane, whereas slow and long vehicles moving in the right lane keep the lane. To simulate this effect, the following lane changing rules have been added to the incentive criteria (29) and (30). A slow vehicle or a long vehicle changes from the left lane to the right lane even if conditions (30) are not satisfied but the condition

$$L \to R: \quad v_n^+ > v_{\text{free}}^{(j)} - \delta_0, \quad j = 2, 3, \tag{33}$$

holds. Here $\delta_0 > 0$ is a constant. A slow vehicle or a long vehicle changes from the right lane to the left lane only if the related condition

$$R \to L: \quad v_{\ell,n} \leqslant v_{\text{free}}^{(j)} - \delta_0, \quad j = 2, 3 \tag{34}$$

is satisfied together with (29). In both cases, the security rules (31) should also be satisfied for lane changing.

If the incentive condition (33) is satisfied for either a slow vehicle or a long vehicle that moves currently in the left (passing) lane but the security rules (31) are not satisfied, then the following conditions are applied. The gap between two neighbouring vehicles in the right lane exceeds some value $g^{(\min)}$, i.e.,

$$x_n^+ - x_n^- - d^+ > g^{(\min)}, \tag{35}$$

$$g^{(\min)} = \lambda v_n^+ + d, \tag{36}$$

where $\lambda = \lambda^{(j)}$, $j = 2, 3$, are constants. In addition, the condition that the vehicle passes the point

$$x_n^{(\text{m})} = \left(x_n^+ + x_n^- + d - d^+\right)/2 \tag{37}$$

between two neighbouring vehicles in the right lane for the time step n should be satisfied, i.e.,

$$\begin{aligned} &x_{n-1} < x_{n-1}^{(\text{m})} \qquad \text{and} \qquad x_n \geqslant x_n^{(\text{m})} \\ &\text{or} \\ &x_{n-1} \geqslant x_{n-1}^{(\text{m})} \qquad \text{and} \qquad x_n < x_n^{(\text{m})}. \end{aligned} \tag{38}$$

If (33) and (35)–(38) are satisfied, the vehicle changes to the right lane and its coordinate is set to $x_n^{(\text{m})}$. Note that the point $x_n^{(\text{m})}$ (37) is chosen from the condition that after lane changing the space gap to the preceding vehicle $x_n^+ - x_n^{(\text{m})} - d^+$ and to the trailing vehicle $x_n^{(\text{m})} - x_n^- - d$ are equal to each other.

Two slow vehicles or two long vehicles moving side by side in the left and right lanes can prevent fast vehicles accelerating in free flow on the two-lane road [48]. To avoid this effect, it is assumed that either a slow vehicle or a long vehicle in the left lane, which should change the lane, can move with a higher maximum speed in free flow until the vehicle changes to the right lane. For this purpose, when (33) is satisfied, the maximum speed v_{free} in (23) for slow or long vehicles in the left lane is

$$v_{\text{free}} = v_{\text{free}}^{(j,\text{left})} > v_{\text{free}}^{(j)}, \qquad j = 2, 3. \tag{39}$$

2.3. Boundary and initial conditions

In the model, 'open' boundary conditions are used. At the start of the road new vehicles are generated one after another in each of the lanes at times

$$t^{(k')} = \tau\lceil k'\tau_{\rm in}/\tau\rceil, \qquad k' = 1, 2, \ldots, \tag{40}$$

where $\tau_{\rm in} = 1/q_{\rm in}$, $q_{\rm in}$ is the flow rate in the incoming boundary flow per lane, $\lceil z\rceil \geqslant z$ denotes the integer nearest to z. A new vehicle appears at time (40) only if the distance from the beginning of the road ($x = x_{\rm b}$) to the position $x = x_{\ell,n}$ of the farthest upstream vehicle in the lane exceeds a safe distance $\ell_{\rm safe} = v_{\ell,n}\tau + d_\ell$. Otherwise, this condition is checked at the time next to $t^{(k')}$ (40), and so on. The speed v_n and coordinate x_n of a new vehicle are $v_n = v_{\ell,n}$ and $x_n = \max(x_{\rm b}, x_{\ell,n} - \max(v_n\tau_{\rm in}, \ell_{\rm safe}))$ respectively.

In the initial state ($n = 0$), all vehicles have the related maximum speed $v_n = v_{\rm free}^{(j)}$, $j = 1, 2, 3$ and they are positioned at space intervals $x_{\ell,n} - x_n = v_{\rm free}^{(j)}\tau_{\rm in}$, $j = 1, 2, 3$. After a vehicle has reached the end of the road it is removed; before this, the farthest downstream vehicle maintains its speed and the lane.

The vehicle type identifier j and the related vehicle parameters are ascribed to the vehicle as its individual 'attributes' when the vehicle is generated at the beginning of the road or it is positioned on the road in the initial state.

In the model, there are two different possibilities of generating vehicles of different types at the start of the road: (i) fast, slow and long vehicles are randomly generated in the left and right lanes with the rates related to given values of the flow rate $q_{\rm in}$ and the percentages $\eta^{(1)}$, $\eta^{(2)}$ and $\eta^{(3)}$. (ii) Fast vehicles are preferably generated in the left lane, whereas slow and long vehicles are preferably generated in the right lane. In the model (ii), only $\max(0, 2\eta^{(1)} - 100\%)$ of fast vehicles are randomly generated in the right lane, whereas only $\max(0, 2\eta^{(2)} + 2\eta^{(3)} - 100\%)$ of slow and long vehicles are randomly generated in the left lane.

2.4. Model of on-ramp bottlenecks

An on-ramp bottleneck is considered. The on-ramp consists of two parts (figure 1(f)): (i) the merging region of the length $L_{\rm m}$ where a vehicle can merge onto the right lane of the main road from the on-ramp. (ii) The on-ramp lane upstream of the merging region (a single-lane road of the length $L_{\rm r}$) where vehicles move according to the model (2)–(16), (19)–(21) with the maximum speed $v_{\rm free,on} = 80$ km h^{-1}. At the beginning of the on-ramp lane $x = x_{\rm on}^{\rm (b)}$ that is upstream of the merging region of the on-ramp the flow rate to the on-ramp $q_{\rm on}$ is given in the same manner as the flow rate on the main road $q_{\rm in}$. Fast, slow and long vehicles are randomly generated depending on the percentages $\eta^{(j)}$, $j = 1, 2, 3$.

Vehicles in the on-ramp lane within the merging region move according to the model rules (2)–(16), (19)–(21). However, in (4)–(6) the coordinate $x_{\ell,n}$ and the speed $v_{\ell,n}$ of the preceding vehicle are replaced by values x_n^+ and $\hat{v}_n^+$, respectively, where

$$\hat{v}_n^+ = \max\bigl(0, \min\bigl(v_{\rm free}, v_n^+ + \Delta v_{\rm r}^{(2)}\bigr)\bigr), \tag{41}$$

x_n^+ and v_n^+ are the coordinate and the speed of the preceding vehicle in the right lane of the main road, $\Delta v_{\rm r}^{(2)}$ is a constant. However, the safe speed in (2) is further determined by the safe speed $v_{{\rm s},n}$ (19) related to the preceding vehicle in the on-ramp lane.

The following rules are used for a vehicle merging onto the main road within the merging region. The rule ($*$): a speed $\hat{v}_n$ is calculated corresponding to the formula

$$\hat{v}_n = \min\bigl(v_n^+, v_n + \Delta v_{\rm r}^{(1)}\bigr), \tag{42}$$

where $\Delta v_{\rm r}^{(1)}$ is a constant that describes the maximum possible increase in the vehicle speed after merging. Then the speed $\hat{v}_n$ is used instead of v_n in the security lane changing rules (31).

If these conditions are satisfied, then the vehicle merges onto the main road. Otherwise, the rule (∗∗) is applied: conditions (35)–(38) should be satisfied where in (36) $\lambda = \lambda^{(\mathrm{on})}$, $\lambda^{(\mathrm{on})}$ is constant. After merging the vehicle changes the speed v_n in accordance with (42). The vehicle coordinate does not change in the case of rule (∗) and it is set to $x_n = x_n^{(\mathrm{m})}$ in the case of rule (∗∗). If neither the rule (∗) nor the rule (∗∗) is satisfied the vehicle does not merge onto the neighbouring (right) lane. In this case, the vehicle moves in the on-ramp lane until it comes to a stop at the end of the merging region.

2.5. Simulation parameters

2.5.1. General parameters. In our simulations, the length of the main road is $L = 40$ km, the point $x = 0$ is at the distance $L/2 = 20$ km from the end of the road so the road starts at $x_{\mathrm{b}} = -L/2 = -20$ km. The general model parameters are: $\tau = 1$ s, $a = 0.5$ m s^{-2}, $\beta = 1$, $p_1 = 0.3$, $\delta = 0.01$, $p_2(v) = 0.48 + 0.32\theta(v - 15)$, $p_{\mathrm{c}} = 0.2$, $\Delta v_{\mathrm{r}}^{(1)} = 10$ m s^{-1}, $\Delta v_{\mathrm{r}}^{(2)} = 5$ m s^{-1}, $x_{\mathrm{on}} = 16$ km, $L_{\mathrm{m}} = 300$ m, $L_{\mathrm{r}} = 2$ km. The on-ramp inflow is switched at $t = t_0 = 7$ min. When other values of model parameters are used for some simulations, they are given in the related figure captions.

2.5.2. Fast, slow and long vehicles. In our simulations, the following model parameters are used for heterogeneous traffic flow: $v_{\mathrm{free}}^{(1)} = 33.3$ m s^{-1} (120 km h^{-1}), $v_{\mathrm{free}}^{(2)} = v_{\mathrm{free}}^{(3)} = 25$ m s^{-1} (90 km h^{-1}), $d^{(1)} = d^{(2)} = 7.5$ m, $d^{(3)} = 17$ m, $k^{(1)} = k^{(2)} = 3$, $k^{(3)} = 4$, $p_{\mathrm{a}}^{(1)} = p_{\mathrm{a}}^{(2)} = 0.17$, $p_{\mathrm{a}}^{(3)} = 0.3$, $p_{\mathrm{b}}^{(1)} = p_{\mathrm{b}}^{(2)} = 0.1$, $p_{\mathrm{b}}^{(3)} = 0.2$. The probabilities $p_0^{(j)}(v)$, $j = 1, 2, 3$, in (26) are $p_0^{(1)}(v) = 0.6 + 0.17 \min(1, v/10))$, $p_0^{(2)}(v_n) = 1 - 1.3\big(1 - p_0^{(1)}(v_n)\big)$, $p_0^{(3)}(v_n) = 1 - 1.5\big(1 - p_0^{(1)}(v_n)\big)$. Lane changing parameters are $\delta_1 = 1$ m s^{-1}, $\delta_2 = 3.5$ m s^{-1} for fast vehicles; $\delta_1 = 3.5$ m s^{-1}, $\delta_2 = 1$ m s^{-1} for slow and long vehicles; $\delta_0 = 6$ m s^{-1}. $\lambda^{(2)} = \lambda^{(3)} = 0.8$; $v_{\mathrm{free}}^{(2,\mathrm{left})} = 28.5$ m s^{-1}, $v_{\mathrm{free}}^{(3,\mathrm{left})} = 27.5$ m s^{-1}. $\lambda^{(\mathrm{on})}$=0.72.

2.5.3. Identical vehicles. In our simulations of the two-lane model of identical vehicles made for a comparison with congested pattern formation in heterogeneous flow, in addition to the above general parameters, the following model parameters are used: $v_{\mathrm{free}} = 30$ m s^{-1} (108 km h^{-1}), $d = 7.5$ m, $k = 3$, $p_{\mathrm{a}} = 0.17$, $p_{\mathrm{b}} = 0.1$, $p_0(v) = 0.575 + 0.125 \min(1, v/10))$. $\delta_1 = \delta_2 = 2$ m s^{-1}. $\lambda^{(\mathrm{on})}$=0.75.

3. Congested patterns at bottlenecks on a two-lane freeway in a flow with identical vehicles

3.1. Types of congested patterns and their diagram

Types of congested patterns on a two-lane freeway and the diagram of these patterns at an on-ramp bottleneck, i.e., the regions of the spontaneous occurrence of the patterns in the flow–flow plane with coordinates q_{in} and q_{on}, are qualitatively the same (figures 2, 3) as those found in [22, 24]. There are two main types of congested patterns: a synchronized flow pattern (SP) and a general pattern (GP).

Different SPs (figures 2(*b*)–(*d*)) occur between the boundaries $F_S^{(B)}$ and $S_J^{(B)}$ in the diagram (figure 2(*a*)). The boundaries $F_S^{(B)}$ and $S_J^{(B)}$ are related to a spontaneous F→S transition and a spontaneous phase transition from synchronized flow to a wide moving jam (S→J transition), respectively. The downstream front of a widening SP (WSP) is fixed at the on-ramp bottleneck (figure 2(*b*)). The upstream front of the WSP is continuously widening upstream. The WSP

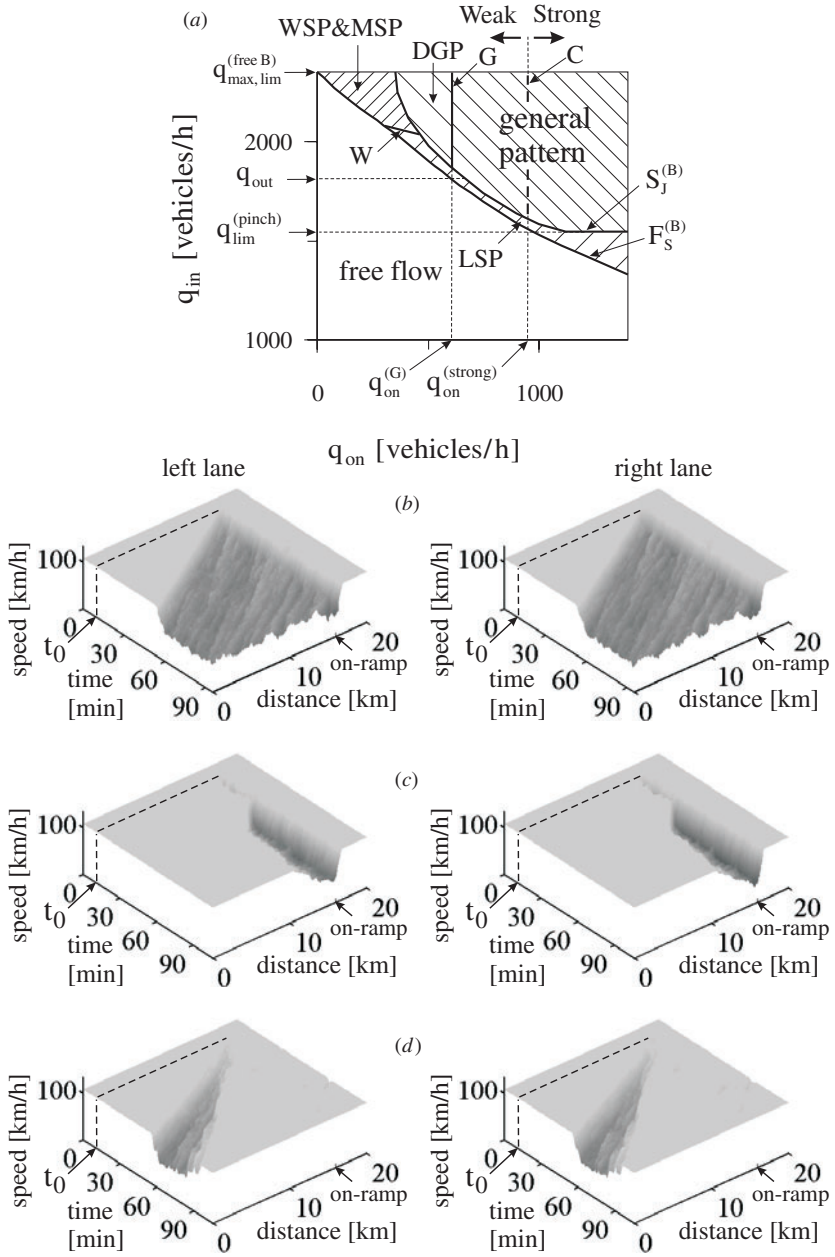

Figure 2. Diagram of congested patterns at an on-ramp bottleneck (*a*) for traffic flow with identical vehicles on a two-lane road and SPs (*b*)–(*d*): (*b*) the widening SP (WSP), (*c*) the localized SP (LSP), (*d*) the moving SP (MSP). In (*b*)–(*d*) the flow rates (q_{on}, q_{in}) are: (*b*) (300, 2250), (*c*) (550, 1846) and (*d*) (25, 2323) vehicles h^{-1}. In (*a*) the criteria for the boundaries $F_S^{(B)}$ and $S_J^{(B)}$ are the same as those in [23]. $q_{max,lim}^{(B)} \approx 2350$ vehicles h^{-1}. $L_m = 500$ m.

occurs above the boundary W in figure 2(*a*). Below the boundary W a localized SP (LSP) occurs. As in WSPs, the downstream front of the LSP is fixed at the bottleneck. However,

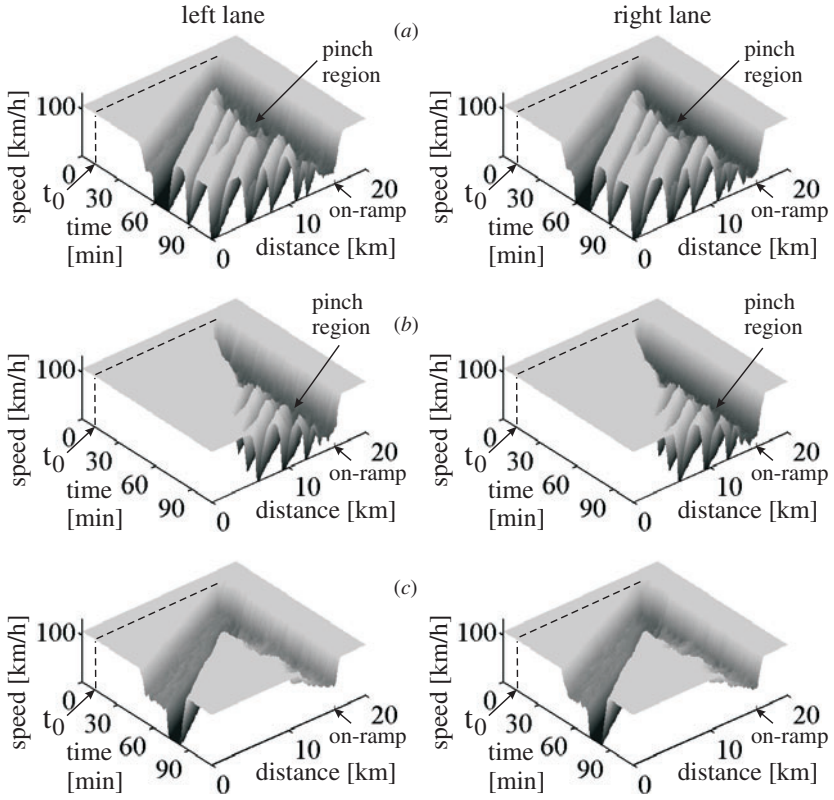

Figure 3. GPs related to the diagram in figure 2(*a*): (*a*) GP at $q_{\text{in}} > q_{\text{out}}$, (*b*) GP at $q_{\text{in}} < q_{\text{out}}$, (*c*) dissolving GP (DGP). The flow rates (q_{on}, q_{in}) are: (*a*) (1000, 2308), (*b*) (1200, 1698) and (*c*) (450, 2308) vehicles h^{-1}.

the upstream front of the LSP is localized at some distance L_{LSP} upstream of the bottleneck (figure 2(*c*)). At higher q_{in} and low q_{on} a moving SP (MSP) can occur (figure 2(*d*)) rather than a WSP appearing. Since an F→S transition is a first-order phase transition, SPs often emerge after some time delay (figure 2(*c*)). Qualitatively the same SPs appear spontaneously in the left and right lanes of the road (figures 2(*b*)–(*d*)).

In the diagram (figure 2(*a*)), right of the boundary G and right of the boundary $S_J^{(B)}$ GPs occur (figure 3). In synchronized flow of a GP the pinch effect, i.e., the self-compression of synchronized flow upstream of the on-ramp, is realized [22]. In the related pinch region of synchronized flow in the GP the density increases and the speed decreases (figures 3(*a*), (*b*)). In the pinch region of a GP, narrow moving jams emerge spontaneously and grow (figures 3(*a*), (*b*)). Some of these narrow moving jams transform into wide moving jams. As a result, upstream of the pinch region of the GP a sequence of wide moving jams appears (figures 3(*a*), (*b*)). Every wide moving jam propagates on the road while maintaining the mean velocity v_{g} of the downstream jam front. This steady propagation of the downstream front of a wide moving jam on the road is represented by the line J in the flow–density plane [55, 56] (figure 1(*b*))[4].

[4] Recall that the left coordinates of the line J are associated with the jam outflow (flow rate and density), the slope of the line J is equal to the mean velocity of the downstream jam front, v_{g}, and the right coordinates of the line J are associated with the state within the jam with the speed $v_{\min} = 0$ and the jam density $\rho_{\max}$.

Right of the boundary $S_J^{(B)}$ and left of the boundary G a dissolving GP (DGP) occurs (figure 3(c)). In the DGP, the pinch region is dissolved after wide moving jam formation and a LSP remains on the main road at the on-ramp bottleneck.

Right to the line C in figure 2(a), i.e., at $q_{\rm on} > q_{\rm on}^{\rm (strong)}$, the strong congestion condition is realized within the pinch region of a GP. In the case of strong congestion, the flow rate $q^{\rm (pinch)}$ in the pinch region reaches a limit value $q^{\rm (pinch)} = q_{\rm lim}^{\rm (pinch)}$, and the frequency of moving jam emergence $f_{\rm narrow}$ reaches a maximum [24]. In contrast, left of the boundary C, i.e., at $q_{\rm on} < q_{\rm on}^{\rm (strong)}$, and right of the boundary $S_J^{(B)}$ the weak congestion condition is realized in a GP. In this case, the pinch region characteristics depend on traffic demand, i.e., on $q_{\rm on}$ [24].

3.2. Single vehicle characteristics in synchronized flow

Small amplitude random fluctuations in synchronized flow destroy hypothetical steady states of synchronized flow [15–18, 20, 21]. These model steady states are only related to a *hypothetical* unperturbed and noiseless vehicle motion that does not occur in reality. Besides fluctuations there are dynamical effects in synchronized flow, which destroy steady states. Examples of these dynamical effects are different driver time delays. These time delays lead to vehicle speed differences. There is a competition of these time delay effects with the speed adaptation effect in synchronized flow [22, 24] that attracts vehicles to a region of small speed differences. Thus, rather than steady states some *dynamical* spatial–temporal synchronized flow states appear after a SP occurs [17, 22, 23]. Examples of these dynamical states of synchronized flow are dependences of the speed and space gap on time for two different vehicles moving through a WSP that occurs at the bottleneck (figures 4(a)–(d)).

Features of dynamical states of synchronized flow found in simulations (figure 4) are correlated with empirical single vehicle data in real traffic flow (e.g., [49–51]). In particular, as in empirical data [49, 50] these dynamical states cover a 2D region in the distance–speed plane (figures 4(e), (f)). In synchronized flow, as in empirical results [51], vehicle acceleration $\alpha_n = (v_n - v_{n-1})/\tau$ and also vehicle speed difference $\delta v_n = v_{\ell,n} - v_n$ (the difference between the speed of the preceding vehicle and the vehicle speed) as functions of time exhibit random jumps and drops in the vicinity of $\alpha_n = 0$ and $\delta v_n = 0$, respectively (figures 4(g)–(j)).

In accordance with an empirical data analysis made by Wagner and Lubashevsky [51], model frequency distributions $p_{\delta v}(\delta v)$ of speed differences between vehicles in synchronized flow have a very sharp maximum at $\delta v = 0$ (figure 5). The above behaviour of frequency distributions $p_{\delta v}(\delta v)$ is valid for different vehicle speeds and space gaps in synchronized flow (figure 5). This attraction of vehicles in synchronized flow to a region with small speed differences is associated with the speed adaptation effect within the synchronization distance. This speed adaptation effect in synchronized flow is a fundamental feature of three-phase traffic theory [21–24].

Simulations show that features of phase transitions in these complex dynamical synchronized flow states (figures 4, 5) are qualitatively the same as those in hypothetical steady states of synchronized flow.

4. Patterns in heterogeneous traffic flow

4.1. Vehicle separation effect in free flow

Due to the existence of fast and slow vehicles, there is the well-known lane specific behaviour in free flow (e.g., [52, 54]): fast vehicles try to change to the left lane (passing lane), whereas

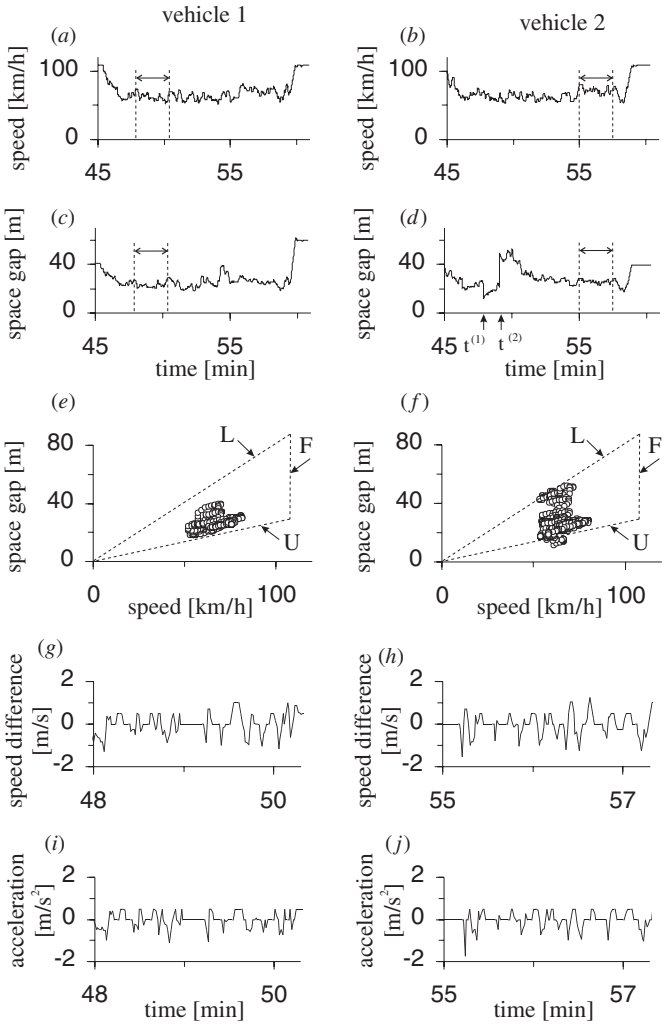

Figure 4. Single vehicle characteristics in synchronized flow within a WSP at an on-ramp bottleneck shown in figure 2(*b*). (*a*)–(*d*) Speed (*a*), (*c*) and space gap (*b*), (*d*) as functions of time for two vehicles moving through the WSP. (*e*), (*f*) Points in the space-gap–speed plane related to (*a*), (*c*) and (*b*), (*d*), respectively. (*g*)–(*j*) Speed difference $\delta v_n = v_{\ell,n} - v_n$ (*g*), (*h*) and vehicle acceleration α_n (*i*), (*j*) related to time intervals marked by arrows in (*a*)–(*d*). Figures (*a*), (*c*), (*e*), (*g*), (*i*) are for vehicle 1 and figures (*b*), (*d*), (*f*), (*h*), (*j*) are for vehicle 2. Vehicle 1 and the related preceding vehicle move in the right lane only. Vehicle 2 starts to move in the left lane, then it changes to the right lane at $t^{(1)} = 48$ min; the related preceding vehicle changes from the right lane to the left lane at $t^{(2)} = 49$ min. The lines F, U and L in (*e*), (*f*) are the boundaries for steady states in the space-gap–speed plane related to the corresponding boundaries for steady states in the flow–density plane in figure 1(*a*).

slow vehicles are required to move in the right lane. As a result, the average speed in the left lane is higher than in the right lane (figure 6).

In figure 6, at the beginning of the road slow and fast vehicles (50% fast and 50% slow vehicles) appear randomly in the left and right lanes with the same mean rate (the method (i) of section 2.3). Firstly, slow vehicles force fast vehicles to move with a lower speed than the

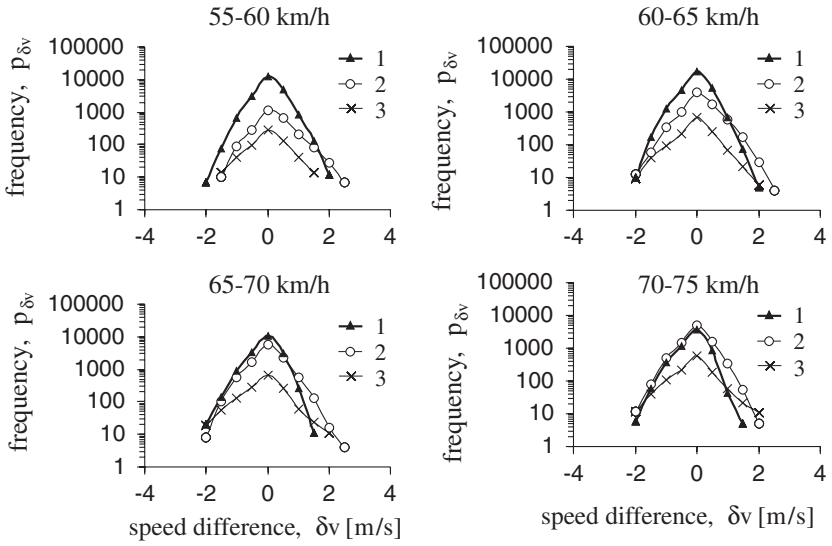

Figure 5. Frequency distributions $p_{\delta v}$ of speed difference δv between two following one another vehicles related to different vehicle speed intervals (indicated in related figures) and different space gap intervals. Data correspond to synchronized flow inside the WSP shown in figure 2(*b*). Space gaps between vehicles are within intervals: 15–25 m (curves 1), 25–35 m (curves 2) and 35–45 m (curves 3).

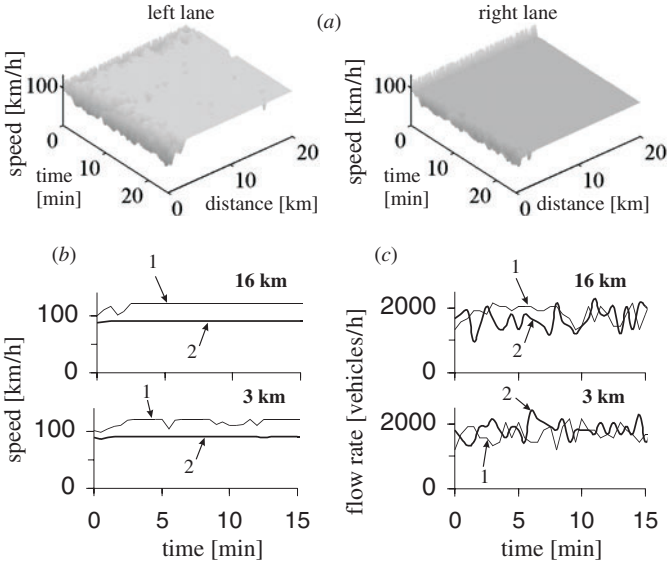

Figure 6. Separation of fast and slow vehicles between the left and right lanes in free flow. (*a*) Speed distributions in time and space in the left and right lanes. (*b*), (*c*) Vehicle speed (*b*) and flow rate (*c*). Curves 1 and 2 in (*b*), (*c*) are related to the left and right lanes, respectively. At the beginning of the road slow and fast vehicles appear randomly in the left and right lanes (method (i) in section 2.3). In the initial state at $n = 0$ fast and slow vehicles have been distributed randomly between the lanes. $\eta^{(1)} = 50\%$, $\eta^{(2)} = 50\%$. $q_{\text{in}} = 1800$ vehicles h^{-1}. The road length is $L = 20$ km. The beginning of the road is located at the point $x_{\text{b}} = 0$.

maximum speed of fast vehicles $v_{\text{free}}^{(1)}$. Therefore, at the beginning of the road the difference between the average speeds in the left and right lanes is low.

Later, fast vehicles change to the left lane. In contrast, slow vehicles have to change to the right lane. This lane changing leads to lane separation of fast and slow vehicles. Beginning at some road location all fast vehicles move with their maximum speed $v_{\text{free}}^{(1)}$ in the left lane and all slow vehicles move with their maximum speed $v_{\text{free}}^{(2)}$ in the right lane. Because $v_{\text{free}}^{(1)} > v_{\text{free}}^{(2)}$ the average speed in the left lane is considerably higher than the average speed in the right lane.

At high flow rates q_{in} large amplitude fluctuations cause a spontaneous emergence of a synchronized flow region near the beginning of the road. However, this is only a model effect that occurs under the boundary conditions for vehicle generation (i) of section 2.3. To diminish this model effect, the boundary conditions for vehicle generation (ii) of section 2.3 are used in all simulations below.

4.2. Onset of congestion in free flow on homogeneous road

If a local perturbation is applied in an initial free flow, then a local region of synchronized flow can occur. Depending on the initial density in free flow and on perturbation characteristics, different states of synchronized flow can be realized due to an F→S transition.

An F→S transition can occur if the flow rate (vehicle density) in an initial free flow is within the range

$$q_{\text{th}} \leqslant q_{\text{in}} \leqslant q_{\text{max}}^{(\text{free})} \qquad \left(\rho_{\text{th}} \leqslant \rho_{\text{in}} \leqslant \rho_{\text{max}}^{(\text{free})}\right), \tag{43}$$

where $\rho_{\text{in}} = q_{\text{in}}/v_{\text{free}}$.

An F→S transition is a first-order phase transition. There is the nucleation effect that governs this phase transition. If a local perturbation occurs within the density range (43) in an initial free flow, then this perturbation grows and leads to the F→S transition only if the amplitude of the perturbation $\Delta v_{\text{initial}}^{(\text{pert})}$ exceeds some critical value $\Delta v_{\text{cr}}^{(\text{FS})}$. Otherwise, the perturbation gradually dissolves and the initial free flow is recovered. There is a threshold density in free flow ρ_{th} (threshold flow rate q_{th}): at the threshold density the amplitude of the perturbation $\Delta v_{\text{cr}}^{(\text{FS})}$ reaches a maximum value. If the density is lower than the threshold density, an F→S transition does not occur. This is regardless of the amplitude of the time-limited local perturbation in free flow. The critical amplitude of the local perturbation $\Delta v_{\text{cr}}^{(\text{FS})}$ is a decreasing function of density in the initial free flow. The above features of the F→S transition are qualitatively the same as those in flow with identical vehicles [22, 24].

However, there is a peculiarity of an F→S transition in heterogeneous traffic flow. If a local perturbation initially appears only in one of the freeway lanes, then the critical amplitude of the local perturbation $\Delta v_{\text{cr}}^{(\text{FS})}$ depends on which of the lanes the perturbation has initially occurred in. At the same flow rate q_{in} in free flow the critical amplitude of a local perturbation in the right lane (curve 1 in figure 7(*a*)) is lower than the critical amplitude of the perturbation in the left lane (curve 2 in figure 7(*a*)). In particular, at the critical point for free flow $q_{\text{max}}^{(\text{free})}$ the critical perturbation amplitude for the left lane $\Delta v_{\text{cr}}^{(\text{FS})} = \Delta v_{\text{cr}}^{(\text{FS,left})}$ (figure 7(*a*), curve 2) is greater than zero, whereas the critical perturbation amplitude for the right lane $\Delta v_{\text{cr}}^{(\text{FS})} = \Delta v_{\text{cr}}^{(\text{FS,right})}$ is zero (curve 1).

As in flow with identical vehicles [24], the threshold point of free flow (ρ_{th}, q_{th}) is related to the condition

$$v_{\text{down}} = v_{\text{up}}, \tag{44}$$

where v_{up} and v_{down} are the velocities of the upstream and downstream fronts of a MSP, respectively (in the case under consideration, we get $v_{\text{up}}, v_{\text{down}} < 0$). In the vicinity of the

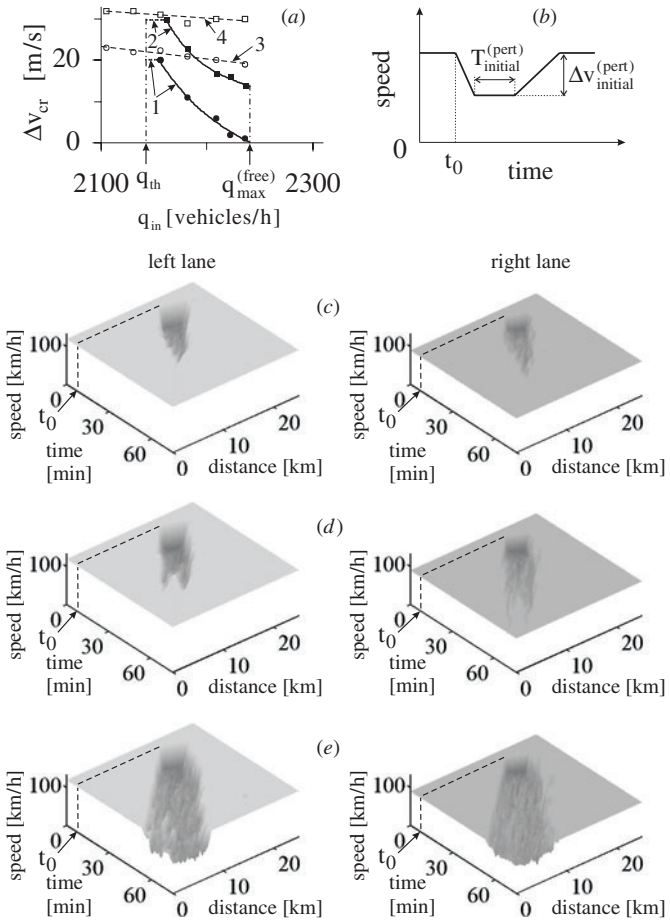

Figure 7. Phase transitions in heterogeneous flow on a homogeneous road. (*a*) Dependences of critical amplitude of a local perturbation for MSP excitation $\Delta v_{\rm cr} = \Delta v_{\rm cr}^{\rm (FS)}$ (curves 1 and 2) and for wide moving jam excitation $\Delta v_{\rm cr} = \Delta v_{\rm cr}^{\rm (FJ)}$ (curves 3 and 4) on the flow rate $q_{\rm in}$. (*b*) Speed of a vehicle that is the source of an initial local perturbation as a function of time. (*c*)–(*e*) Time–space evolution of the initial local perturbation at $q_{\rm in} < q_{\rm th}$ (*c*), $q_{\rm in} = q_{\rm th}$ (*d*) and $q_{\rm in} > q_{\rm th}$ at $\Delta v_{\rm initial}^{\rm (pert)} > \Delta v_{\rm cr}^{\rm (FS)}$ (*e*). In (*a*) curves 1, 3 and curves 2, 4 are related to initial perturbations in the right and left lanes, respectively. $T_{\rm initial}^{\rm (pert)} = 10$ s for the solid parts of curves 1 and 2 in (*a*). In (*c*)–(*e*) $T_{\rm initial}^{\rm (pert)} = 180$ s, the inflow rate $q_{\rm in}$ is: (*c*) 2117, (*d*) 2145, (*e*) 2200 vehicles h^{-1}. $\eta^{(1)} = 50\%$, $\eta^{(2)} = 50\%$.

threshold point, the duration of an initial perturbation $T_{\rm initial}^{\rm (pert)}$ (figure 7(*b*)) should be increased for F→S transition occurrence (dashed parts of curves 1 and 2 in figure 7(*a*)) in comparison with a constant duration $T_{\rm initial}^{\rm (pert)} = 10$ s used for the solid parts of curves 1 and 2 in figure 7(*a*). $T_{\rm initial}^{\rm (pert)}$ increases when the flow rate $q_{\rm in}$ decreases.

At $q_{\rm in} < q_{\rm th}$ we have $|v_{\rm down}| > |v_{\rm up}|$. As a result, no F→S transition can occur (figure 7(*c*)). At the threshold point where condition (44) is satisfied, a MSP can be excited by application of a local perturbation. The downstream and upstream fronts of the MSP move with the same mean velocities (figure 7(*d*)). However, at the threshold point of free flow models fluctuations within synchronized flow of the MSP can lead over time to a return

S→F transition. Consequently, the MSP disappears (figure 7(*d*)). When $q_{\rm in} > q_{\rm th}$ and $\Delta v_{\rm initial}^{\rm (pert)} \geqslant \Delta v_{\rm cr}^{\rm (FS)}$, an F→S transition occurs and an MSP emerges where $|v_{\rm down}| < |v_{\rm up}|$ (figure 7(*e*)). The MSP width increases continuously over time.

However, if the amplitude of an initial perturbation $\Delta v_{\rm initial}^{\rm (pert)}$ applied to free flow exceeds $\Delta v_{\rm cr}^{\rm (FS)}$ appreciably, then instead of an MSP a wide moving jam can be formed in synchronized flow of the incipient MSP. This induced F→J transition occurs if the amplitude of an external local perturbation $\Delta v_{\rm initial}^{\rm (pert)}$ in free flow is equal to or exceeds the critical amplitude $\Delta v_{\rm cr}^{\rm (FJ)}$ (figure 7(*a*), curves 3, 4). The critical amplitude for the left lane $\Delta v_{\rm cr}^{\rm (FJ)} = \Delta v_{\rm cr}^{\rm (FJ,left)}$ (curve 4) is greater than the critical amplitude for the right lane $\Delta v_{\rm cr}^{\rm (FJ)} = \Delta v_{\rm cr}^{\rm (FJ,right)}$ (curve 3). If $\Delta v_{\rm initial}^{\rm (pert)} \geqslant \Delta v_{\rm cr}^{\rm (FJ)}$, then first synchronized flow begins to form in free flow and later a wide moving jam emerges spontaneously in that synchronized flow. Thus, wide moving jam emergence is related to a sequence of F→S→J transitions.

4.3. Lane 'asymmetric' emergence of moving synchronized flow patterns

Let us assume that the density is higher than the threshold density of free flow. We consider a subsequent development of an initial local perturbation that occurs only in the right lane. The amplitude of this perturbation is assumed to be slightly greater than the critical amplitude for this lane $\Delta v_{\rm cr}^{\rm (FS,right)}$. In this case, an F→S transition occurs first only in the right lane. As a result, an MSP appears in the right lane (figure 8(*b*)), whereas in the left lane vehicles move with the free flow speed (figures 8(*a*), (*c*)).

Because the speed in the right lane sharply decreases inside the MSP, some of the slow vehicles try to change lane. As a result, over time the speed in the left lane also decreases. This leads to the self-formation of an MSP in both lanes. This is due to the effect of synchronization of the speed between different lanes in synchronized flow.

This lane 'asymmetric' MSP emergence is caused by the different driver behavioural characteristics in heterogeneous traffic flow. However, after the effect of the speed synchronization between different lanes has occurred, qualitative features and spatial–temporal structure of the MSP are the same as those for the MSP in flow with identical vehicles (figures 8(*c*), (*d*); $x = 5$ km and $x = 0$ km) [22].

If an initial local perturbation appears in the left lane only and the perturbation amplitude is greater than the critical amplitude for an F→S transition, then the speed synchronization effect occurs very quickly. In this case, there is almost no time delay in MSP formation in the left and right lanes (figures 8(*e*), (*f*)). When the speed begins to decrease in the left lane, fast vehicles in the region of the lower speed try to change to the right lane where the speed is higher. This synchronizes the average speeds between the lanes and leads to MSP emergence in both lanes (figures 8(*e*), (*f*)). Also in this case, after the MSP is formed in both lanes features of this MSP are qualitatively the same as those of the MSP in flow with identical vehicles.

4.4. Diagram of congested patterns at on-ramp bottlenecks

Types of congested patterns and their diagram at an on-ramp bottleneck in heterogeneous flow with fast and slow vehicles (figures 9 and 10) are qualitatively similar to those for identical vehicles (figures 2 and 3). The same three types of synchronized flow patterns, WSPs, LSPs and MSPs (figures 9(*b*)–(*d*)), can occur spontaneously between the boundaries $F_S^{(B)}$ and $S_J^{(B)}$ in the diagram (figure 9(*a*)). Inside a WSP, a LSP and a MSP the speed is appreciably synchronized across the lanes (figures 11(*a*), (*c*), (*e*)). However, at the downstream front of all these SPs at which vehicles accelerate from synchronized flow to free flow downstream the

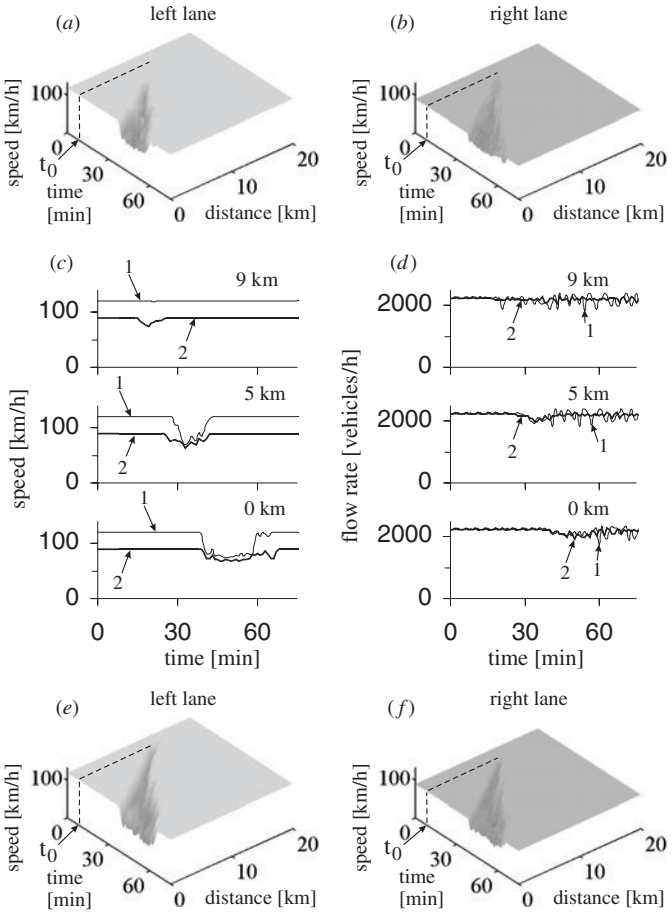

Figure 8. MSP on a homogeneous road excited by a local perturbation. (*a*), (*b*) Speed distribution in time and space for MSP excited by a local perturbation in the right lane. (*c*), (*d*) Vehicle speed (*c*) and flow rate (*d*) for MSP in (*a*), (*b*). (*e*), (*f*) Speed distribution in time and space for MSP excited by a local perturbation in the left lane. In (*c*), (*d*) one minute average data of virtual detectors are shown, curves 1 and 2 are related to the left and right lanes, respectively. $q_{\text{in}} = 2230$ vehicles h^{-1}. $\eta^{(1)} = 50\%$, $\eta^{(2)} = 50\%$. The initial local perturbation (figure 7(*b*)) with amplitude $\Delta v_{\text{initial}}^{(\text{pert})} = 5$ m s^{-1} (*a*)–(*d*) and $\Delta v_{\text{initial}}^{(\text{pert})} = 20$ m s^{-1} (*e*), (*f*) and duration $T_{\text{initial}}^{(\text{pert})} = 1$ s is applied at $t_0 = 7$ min at the location $x = 11$ km.

effect of the vehicle separation occurs (section 4.1). For this reason, in free flow downstream of SPs there is a large difference between the average vehicle speeds in the left and right lanes (figures 11(*a*), (*c*), (*e*)).

Similar to the pattern diagram for the identical vehicles (figure 2(*a*)), in the pattern diagram for heterogeneous flow shown in figure 9(*a*), right of the boundary G and right of the boundary $S_J^{(B)}$ a GP occurs. In the GP, the pinch region exists continuously where narrow moving jams emerge spontaneously. Some of these narrow moving jams transform into wide moving jams. As a result, a sequence of wide moving jams propagating upstream appears (figures 10(*a*), (*b*)).

Right of the boundary $S_J^{(B)}$ and left of the boundary G a dissolving GP (DGP) occurs (figure 10(*c*)). In the DGP, the pinch region is dissolved after wide moving jam formation. As

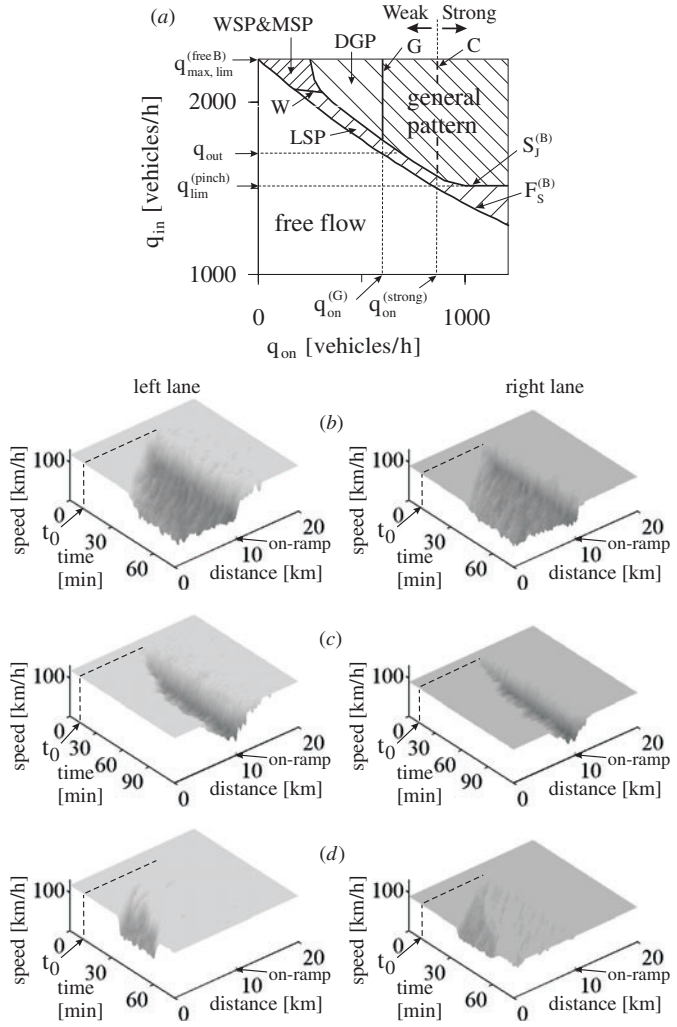

Figure 9. Diagram of congested patterns at an on-ramp bottleneck in heterogeneous traffic flow with fast and slow vehicles (*a*) and related SPs (*b*)–(*d*): (*b*) WSP, (*c*) LSP, (*d*) MSP. In (*b*)–(*d*) the flow rates (q_{on}, q_{in}) are: (*b*) (200, 2195), (*c*) (400, 1895) and (*d*) (35, 2235) vehicles h^{-1}. $\eta^{(1)} = 50\%$, $\eta^{(2)} = 50\%$. In (*a*) the criteria for the boundaries $F_S^{(B)}$ and $S_J^{(B)}$ are the same as those in [23]. $q_{max,lim}^{(B)} \approx 2250$ vehicles h^{-1}. $x_{on} = 10$ km.

in the case of SPs (figures 9(*b*)–(*d*)), at the downstream front of GPs (figures 10(*a*), (*b*)) and the DGP (figure 10(*c*)) the vehicle separation effect occurs.

At high flow rate on the main road and a low flow rate to the on-ramp, MSPs can occur spontaneously at the bottleneck (figure 9(*d*)). Often an MSP appears first only in the right lane, whereas in the left lane vehicles move at the free flow speed. The physics of this lane 'asymmetric' MSP emergence is the same as for the case of 'asymmetric' MSP emergence on a homogeneous road. Over time some of the slow vehicles moving in the right lane change to the left lane where the speed is higher. As a result, after a time delay an MSP occurs in both the lanes.

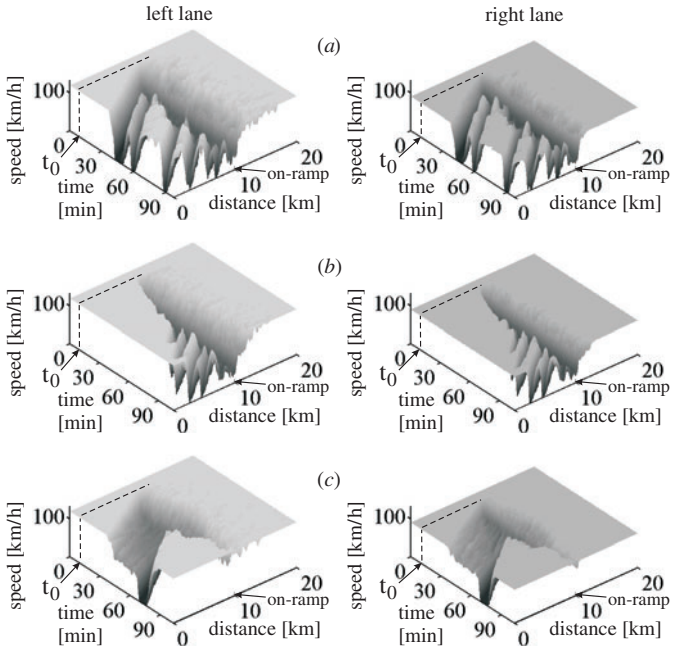

Figure 10. GPs related to the diagram in figure 9(*a*): (*a*) GP at $q_{\text{in}} > q_{\text{out}}$, (*b*) GP at $q_{\text{in}} < q_{\text{out}}$, (*c*) dissolving GP (DGP). The flow rates $(q_{\text{on}}, q_{\text{in}})$ are: (*a*) (850, 2180), (*b*) (1250, 1600) and (*c*) (360, 2195) vehicles h^{-1}. $x_{\text{on}} = 10$ km.

It should be noted that this time delay in MSP formation in the left lane is a random effect. In other realizations at the same initial conditions it can turn out that the MSP occurs almost simultaneously in both lanes. To explain this, note that during MSP formation in the right lane there are some fast vehicles that merge onto the right lane of the main road from the on-ramp. These fast vehicles have to move with a lower speed in the right lane inside the incipient MSP. When these fast vehicles change to the left lane, then due to their low initial speed they decrease the speed in the left lane. This leads to MSP emergence in both lanes.

Inside the 'synchronized flow' and 'wide moving jam' phases, i.e., in congested traffic there is no complete separation of fast and slow vehicles between the left and right lanes, respectively. Inside synchronized flow where the average speed is lower than the maximum speed for slow vehicles, fast vehicles can change to the right lane and slow vehicles can change to the left lane (figure 12). This lane changing depends on the current difference between vehicle speeds in these lanes: fast and slow vehicles change to the lane where the speed is currently higher. This decreases the difference between the average speeds in the left and right lanes, i.e., this intensifies the speed synchronization effect.

The lower the average speed in synchronized flow, the higher the percentage of fast vehicles that move in the right lane. In particular, in SPs only about 5% of fast vehicles move on average in the right lane and about 5% of slow vehicles move in the left lane. In GPs where the average speed is lower than inside SPs, we obtain that about 20% of fast vehicles move in the right lane and about 20% of slow vehicles move in the left lane (figure 12).

In heterogeneous traffic flow with 50% of fast vehicles and 50% of slow vehicles, the limit flow rate in the pinch region of a GP under the strong congestion condition [24] $q_{\text{lim}}^{(\text{pinch})}$ is approximately 1540 vehicles h^{-1}. This limit flow rate is close to the value $q_{\text{lim}}^{(\text{pinch})} =$ 1520 vehicles h^{-1} in flow of identical vehicles. However, the maximum flow rate in free

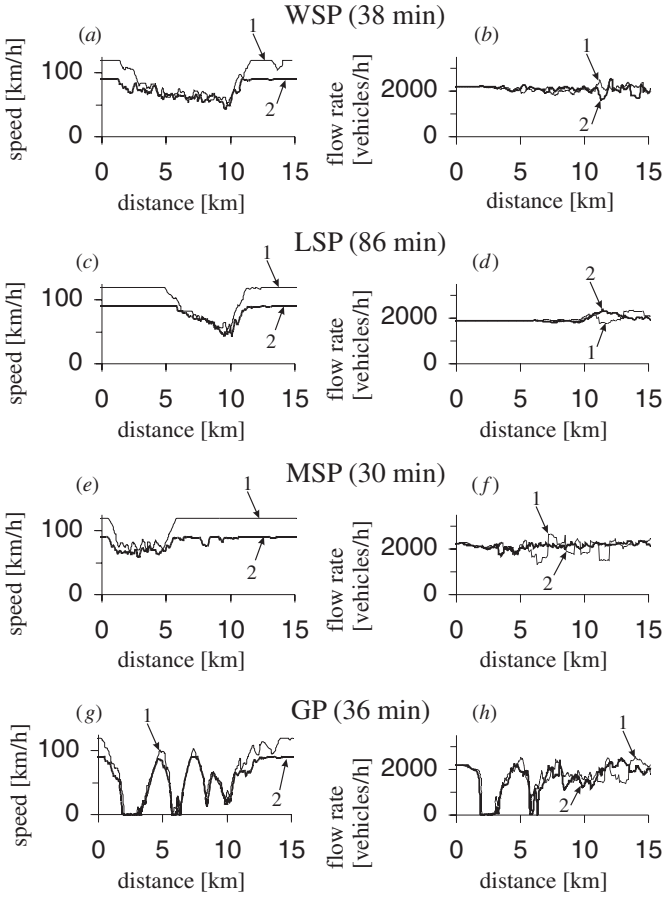

Figure 11. Space distribution of vehicle speed (*a*), (*c*), (*e*), (*g*) and flow rate (*b*), (*d*), (*f*), (*h*) at given times for a WSP (*a*), (*b*), a LSP (*c*), (*d*), a MSP (*e*), (*f*) and a GP (*g*), (*h*). Figures (*a*), (*b*) correspond to the WSP shown in figures 9(*b*); (*c*), (*d*) to the LSP in figures 9(*c*); (*e*), (*f*) to the MSP in figure 9(*d*) and (*g*), (*h*) to the GP in figure 10(*a*). In (*a*), (*c*), (*e*), (*g*) single vehicle data are used for speed distributions, for flow rate distributions the data are averaged over 30 vehicles for SPs (*b*), (*d*), (*f*) and over 10 vehicles for the GP (*h*). Curves 1 and 2 are related to the left and right lanes, respectively.

flow on the main road $q_{\mathrm{max,lim}}^{(\mathrm{free\,B})} = 2250$ vehicles h^{-1} downstream at the on-ramp bottleneck in this heterogeneous traffic flow is appreciably less than the related maximum flow rate for flow with identical vehicles $q_{\mathrm{max,lim}}^{(\mathrm{free\,B})} = 2350$ vehicles h^{-1}. Also the flow rate in the outflow from a wide moving jam $q_{\mathrm{out}} \approx 1725$ vehicles h^{-1} for the case when free flow is formed in the jam outflow in the heterogeneous traffic flow is less than the related flow rate $q_{\mathrm{out}} = 1810$ vehicles h^{-1} in flow with identical vehicles.

This decrease in the maximal flow rate $q_{\mathrm{max,lim}}^{(\mathrm{free\,B})}$ in heterogeneous flow is because the maximal speed of slow vehicles $v_{\mathrm{free}}^{(2)}$ is lower than the maximum speed of identical vehicles v_{free} and the time delay in vehicle acceleration at the downstream front of a wide moving jam for slow vehicles $\tau_{\mathrm{del}}^{(\mathrm{a},2)}(0)$ is greater than this time delay for identical vehicles $\tau_{\mathrm{del}}^{(\mathrm{a})}(0)$.

When heterogeneous traffic flow consists of fast vehicles and long vehicles, an F→S transition and congested pattern features are qualitatively similar to the features considered

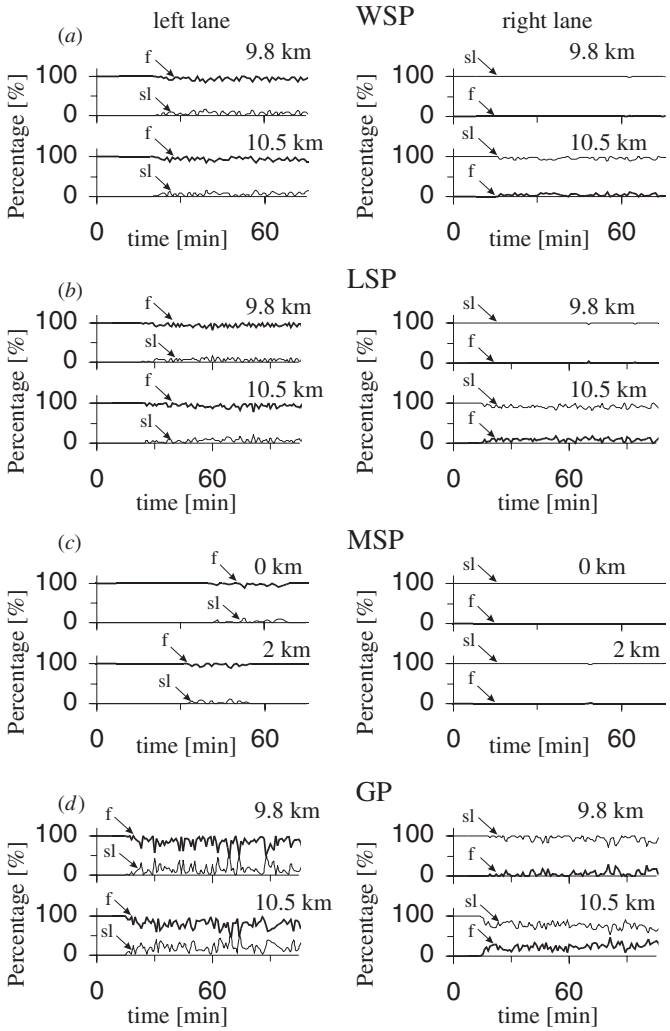

Figure 12. Percentages of fast (curves f) and slow vehicles (curves sl) in the left and right lanes: (*a*) WSP, (*b*) LSP, (*c*) MSP, (*d*) GP. Figures (*a*)–(*c*) are related to the SPs shown in figures 9(*b*)–(*d*), respectively. (*d*) Corresponds to the GP in figure 10(*a*). In (*a*)–(*d*) one minute average data of virtual detectors are shown.

above in heterogeneous traffic flow with different driver behavioural characteristics where all vehicles have the same length. In particular, when traffic flow consists of 50% fast vehicles and 50% long vehicles there are qualitatively the same first-order F→S transitions leading to the onset of congestion in initial free flow, the same types of congested patterns and the same pattern diagram at an on-ramp bottleneck (figures 13 and 14) as those discussed above for heterogeneous flow with fast and slow vehicles.

4.5. Wide moving jam propagation

It has been found that after a wide moving jam has been formed at the upstream boundary of the pinch region within a GP, wide moving jam propagation in heterogeneous flow

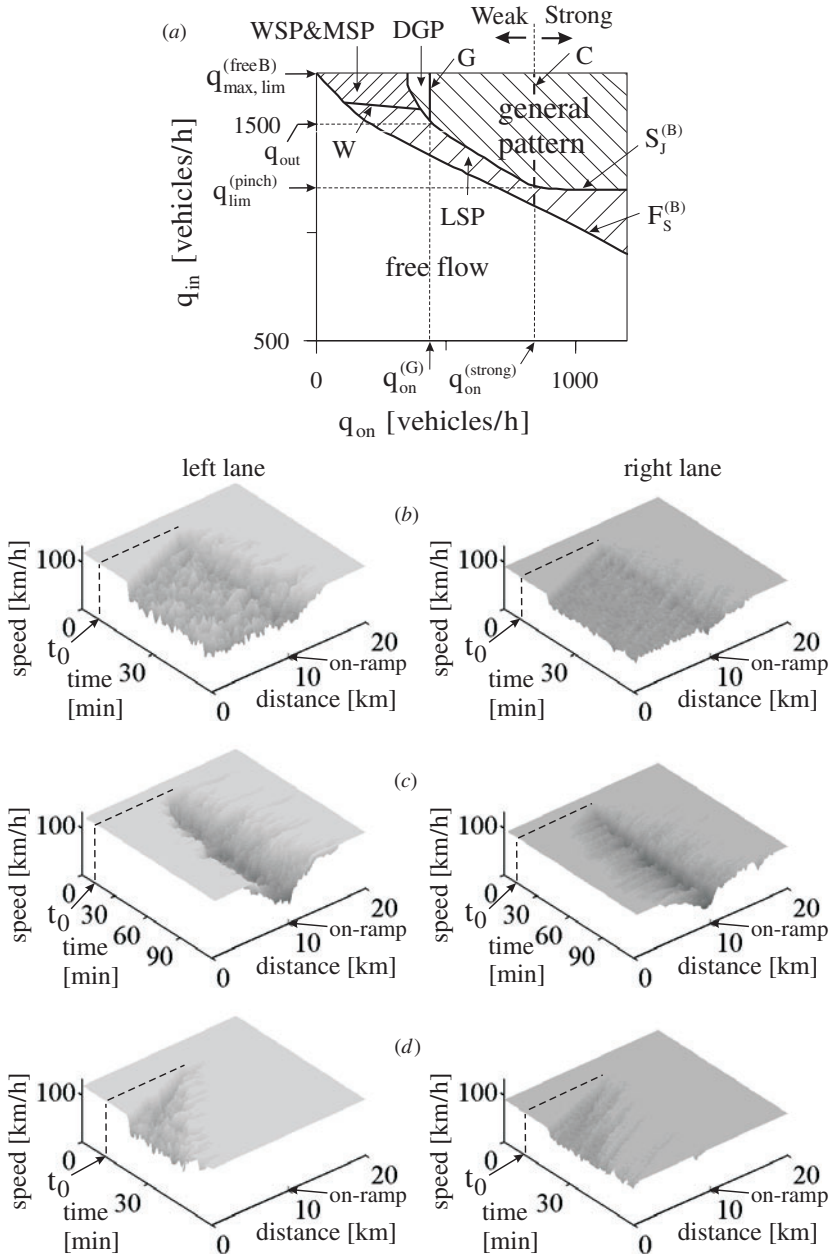

Figure 13. Diagram of congested patterns in heterogeneous flow with fast and long vehicles (*a*) and related SPs (*b*)–(*d*): (*b*) WSP, (*c*) LSP, (*d*) MSP. In (*b*)–(*d*) the flow rates ($q_{\rm on}$, $q_{\rm in}$) are: (*b*) (150, 1740), (*c*) (400, 1470) and (*d*) (15, 1740) vehicles $\rm h^{-1}$. $\eta^{(1)} = 50\%$, $\eta^{(3)} = 50\%$. $q^{(\rm freeB)}_{\rm max,lim} \approx 1740$ vehicles $\rm h^{-1}$. $\lambda^{(\rm on)} = 0.55$.

(figures 15(*a*), (*b*)) has a peculiarity in comparison with wide moving jam propagation in flow with identical vehicles. During wide moving jam propagation, there are time intervals when the downstream front of the jam in the left lane moves with a more negative velocity than the velocity of the downstream front of the jam in the right lane (figures 15(*a*), (*b*),

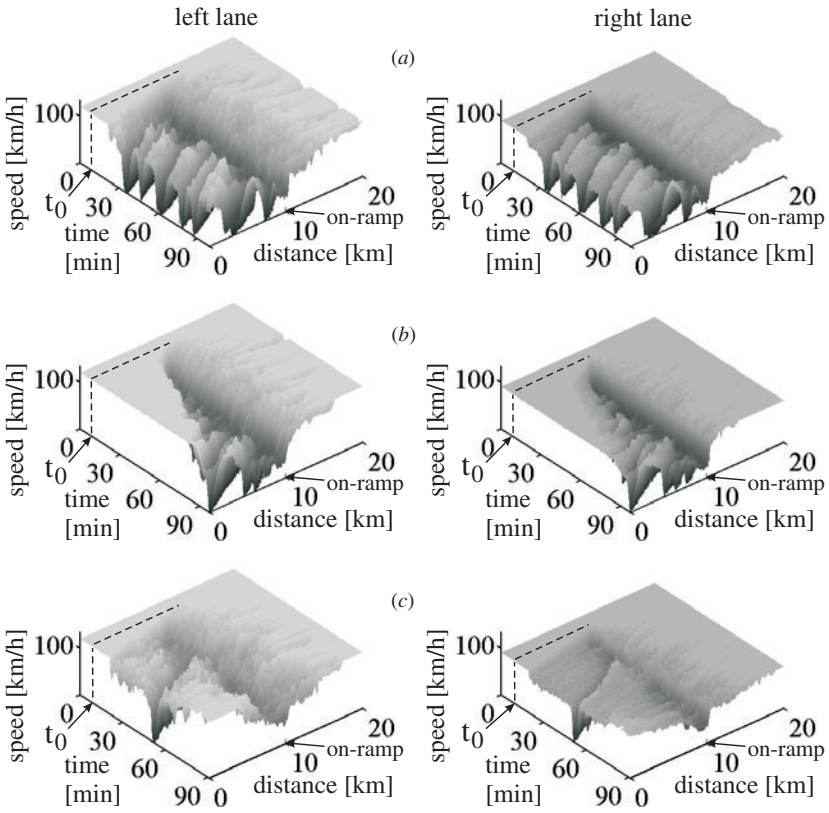

Figure 14. GPs related to the diagram in figure 13(*a*): (*a*) GP at $q_{\rm in} > q_{\rm out}$. (*b*) GP at $q_{\rm in} < q_{\rm out}$. (*c*) DGP. The flow rates $(q_{\rm on}, q_{\rm in})$ are: (*a*) (1000, 1714), (*b*) (1150, 1310) and (*c*) (360, 1714) vehicles h^{-1}.

$t = 84$ min). As a result, at lower speeds within these time intervals the jam fronts do not coincide with one another (one of the distances between the fronts is denoted by $\ell^{(\mathrm{J})}_{\rm down}$ in figure 15(*a*), $t = 84$ min). However, within other time intervals the difference between locations of the downstream jam fronts in the left and right lanes is not observed (figure 15(*a*), $t = 83$ and 85 min). This behaviour can be explained as follows.

The time delay in acceleration of fast vehicles at the downstream front of a wide moving jam $\tau^{(\mathrm{a},1)}_{\rm del}(0)$ is lower than the time delay for slow vehicles:

$$\tau^{(\mathrm{a},1)}_{\rm del}(0) < \tau^{(\mathrm{a},2)}_{\rm del}(0). \tag{45}$$

If traffic flow consists of fast vehicles only, then the velocity of the downstream jam front is

$$v^{(1)}_{\rm g} = -\frac{1}{\tau^{(\mathrm{a},1)}_{\rm del}(0)\rho^{(1)}_{\rm max}}, \tag{46}$$

where $\rho^{(1)}_{\rm max} = 1/d^{(1)}$. If traffic flow consists of slow vehicles only, then this velocity is

$$v^{(2)}_{\rm g} = -\frac{1}{\tau^{(\mathrm{a},2)}_{\rm del}(0)\rho^{(2)}_{\rm max}}, \tag{47}$$

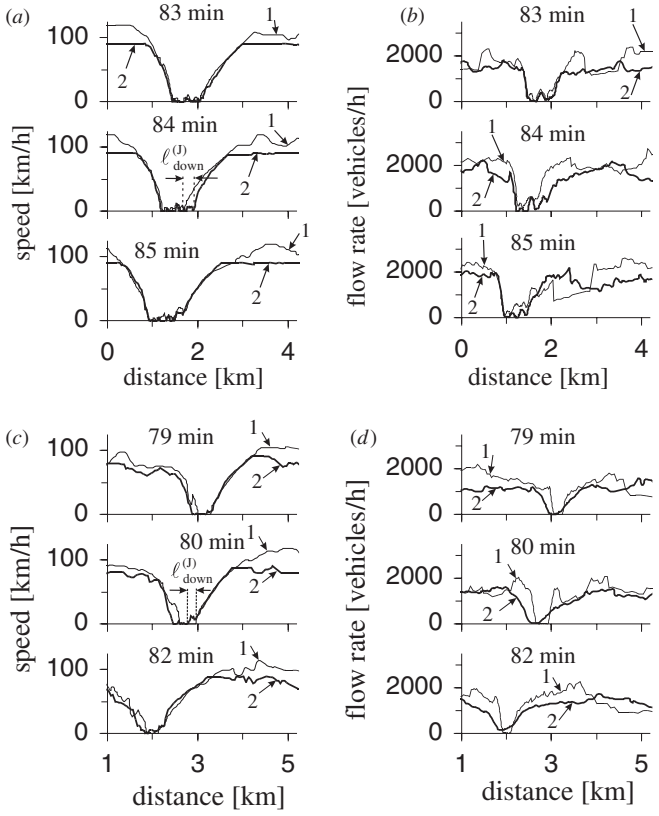

Figure 15. Wide moving jam propagation in heterogeneous flow with fast and slow vehicles (*a*), (*b*) and in heterogeneous flow with fast and long vehicles (*c*), (*d*). Space distributions of vehicle speed (*a*) and flow rate (*b*) at three subsequent times for the wide moving jam that is the third jam in the GP in figure 10(*a*). Space distributions of vehicle speed (*c*) and flow rate (*d*) for a wide moving jam that is the fourth jam in the GP in figure 14(*a*). Curves 1 and 2 are related to the left and the right lanes, respectively. $\ell^{(J)}_{down}$ is the distance between positions of the downstream jam fronts in the left and right lanes. In (*a*), (*c*) single vehicle data are used for speed distributions; data for flow rate distributions (*b*), (*d*) are averaged over 10 vehicles.

where $\rho^{(2)}_{max} = 1/d^{(2)}$. In the model, $d^{(1)} = d^{(2)}$. Thus, corresponding to the condition (45), we obtain

$$\left|v^{(1)}_g\right| > \left|v^{(2)}_g\right|. \tag{48}$$

Although inside a wide moving jam fast and slow vehicles are in both lanes, the fraction of fast vehicles in the left lane is greater than the fraction of slow vehicles. This together with (48) can explain the difference in the velocities of the downstream jam front in the left and right lanes.

When the downstream jam front in the left lane is upstream of this front in the right lane, both fast and slow vehicles try to change to the left lane within the downstream jam front. This lane changing increases the density in the left lane and decreases the speed in this lane. This equalizes the positions of the downstream jam fronts in the lanes (figure 15(*a*), $t = 83$ and 85 min). Later, a lower time delay in acceleration of fast vehicles can cause a quicker upstream propagation of the downstream jam front in the left lane once more. Then due to the above lane changing these front velocities are equalized, and so on. Due to this competition

of the lane changing and the effect of a lower time delay in acceleration of fast vehicles, the downstream front of the wide moving jam propagates on average with the same mean characteristic velocity in the left and right lanes (a general discussion of this effect appears in section 6). This mean velocity does not change over time. This velocity is also the same for different wide moving jams.

It should be noted that after vehicles have accelerated from a wide moving jam to free flow downstream of the jam, the separation of slow and fast vehicles occurs (section 4.1). As a result, the speed in the left lane is higher than the speed in the right lane (figure 15(*a*)). However, this vehicle separation does not complete when synchronized flow is realized between moving jams (see the spatial speed distribution between moving jams shown in figure 11(*g*)).

Wide moving jam propagation in heterogeneous traffic flow with fast and slower long vehicles exhibits some peculiarities (figure 15(*c*), (*d*)). There are time intervals when for lower vehicle speeds the downstream jam front in the right lane is upstream of the downstream jam front in the left lane (figure 15(*c*), $t = 80$ min). To understand this jam propagation behaviour, note that if traffic flow consists of long vehicles only, then the velocity of the downstream jam front is

$$v_{\rm g}^{(3)} = -\frac{1}{\tau_{\rm del}^{({\rm a},3)}(0)\rho_{\rm max}^{(3)}}, \tag{49}$$

where $\rho_{\rm max}^{(3)} = 1/d^{(3)}$. Although $\tau_{\rm del}^{({\rm a},1)}(0) < \tau_{\rm del}^{({\rm a},3)}(0)$, nevertheless due to the condition $d^{(1)} < d^{(3)}$ we get

$$\left|v_{\rm g}^{(1)}\right| < \left|v_{\rm g}^{(3)}\right|. \tag{50}$$

Because the fraction of long vehicles in the right lane is greater than the fraction of fast vehicles, the velocity of the downstream jam front in the right lane is more negative than the one in the left lane. This explains the mentioned difference in downstream jam front propagation in the right and left lanes. However, during the time intervals when the downstream front of the jam in the right lane is upstream of this front in the left lane both fast and long vehicles in the left lane try to change to the right lane. This lane changing increases the density in the right lane and decreases the speed in this lane. This equalizes the positions of the front in the lanes (figure 15(*c*), $t = 79$ and 82 min).

In general, the mean velocity $v_{\rm g}$ of the downstream front of a wide moving jam depends on the relations between the percentages of fast vehicles $\eta^{(1)}$, slow vehicles $\eta^{(2)}$, and long vehicles $\eta^{(3)}$ in heterogeneous flow (see section 6). For the chosen model parameters in figure 9, the velocity $v_{\rm g} = -14.8$ km h^{-1} satisfies the condition $\left|v_{\rm g}^{(2)}\right| < |v_{\rm g}| < \left|v_{\rm g}^{(1)}\right|$. For the chosen model parameters in figure 13, the velocity $v_{\rm g} = -21.9$ km h^{-1} satisfies the condition $\left|v_{\rm g}^{(1)}\right| < |v_{\rm g}| < \left|v_{\rm g}^{(3)}\right|$.

Let us emphasize a qualitative difference between the propagation of the downstream front of a wide moving jam and the propagation of the downstream front of an MSP. It can be seen in figures 8(*a*), (*b*), (*e*), (*f*), 9(*d*) that the velocities of the downstream fronts of these MSPs are not some constant values. For two different MSPs in figures 8(*a*), (*b*), (*e*), (*f*) the related velocities are different as well. Moreover, the velocities of the downstream fronts of the MSPs strongly depend on time when these MSPs propagate on the road. This behaviour of the MSPs is qualitatively different from the wide moving jam propagation. In the latter case, the mean velocity of the downstream front of a wide moving jam is a characteristic parameter that does not depend on time. This parameter is the same for different wide moving jams. This conclusion is true both for traffic flow with identical vehicles and for heterogeneous traffic flow.

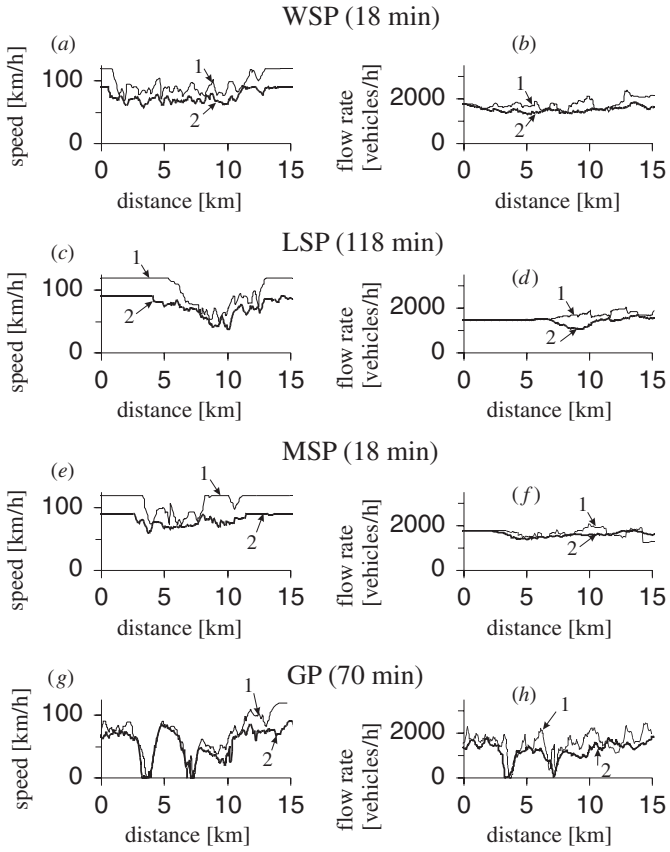

Figure 16. Space distributions of vehicle speed (*a*), (*c*), (*e*), (*g*) and flow rate (*b*), (*d*), (*f*), (*h*) for WSP (*a*), (*b*), LSP (*c*), (*d*), MSP (*e*), (*f*) and GP (*g*), (*h*). (*a*), (*b*) correspond to the WSP shown in figures 13(*b*), (*c*), (*d*) to the LSP in figure 13(*c*), (*e*), (*f*) to the MSP in figure 13(*d*), and (*g*), (*h*) to the GP in figure 14(*a*). In (*a*), (*c*), (*e*), (*g*) single vehicle data are used for speed distributions, for flow rate distributions the data are averaged over 30 vehicles for SPs (*b*), (*d*), (*f*) and over 10 vehicles for the GP (*h*). Curves 1 and 2 are related to the left and right lanes, respectively.

4.6. Partial destroying of speed synchronization

Considering heterogeneous flow with fast and slow long vehicles, it has been found that in SPs of a higher synchronized flow speed, the average speed in the left lane is appreciably higher than that in the right lane (figures 16(*a*), (*c*), (*e*)). Moreover, there are high amplitude oscillations of the speed over time in the left lane (figures 16(*a*), (*e*)). There are also time intervals when the speed in the left lane becomes higher than the maximum speed of long vehicles. This partial destruction of speed synchronization occurs because at a higher speed conditions for lane changing of long vehicles from the right lane to the left lane are more difficult to satisfy.

To explain this, note that when in synchronized flow the speed in the left lane is higher than the speed in the right lane, long vehicles try to change to the left lane. However, there should be large space gaps in synchronized flow in the left lane for this lane changing. This is because of the large length of long vehicles. As a result, the security conditions for lane changing of long vehicles to the left lane are seldom satisfied. For this reason, fast vehicles can

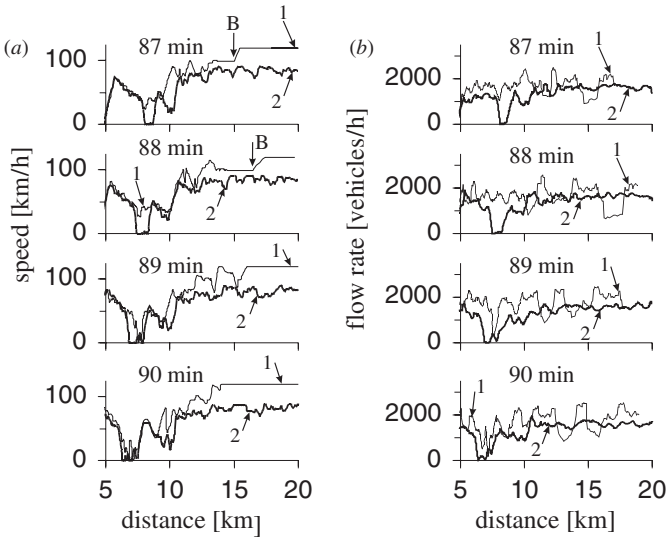

Figure 17. Blocking effect in heterogeneous traffic flow. Arrows B show positions of a long vehicle in the left lane at two times $t = 87$ min and $t = 88$ min. Space distributions of vehicle speed (a) and flow rate (b) for the GP in figure 14(a). Curves 1 and 2 are related to the left and right lanes, respectively. $\eta^{(1)} = 50\%$, $\eta^{(3)} = 50\%$. In (a)–(c) the single vehicle data are used for speed distributions, and the data for flow rate distributions are averaged over 10 vehicles.

accelerate more frequently in the left lane. This leads to an increase in the average speed in the left lane. However, some long vehicles can nevertheless change to the left lane in synchronized flow. This decreases the average speed in the left lane and maintains synchronized flow in both lanes. The lower the average speed in synchronized flow, the lower the difference between the average speeds in the left and right lanes (figure 16(g)).

A destruction of speed synchronization in the left and right lanes can also occur during wide moving jam formation in a GP (figure 17, $t = 87$ and 88 min). In this case, there can be a random time delay in moving jam emergence in the left lane after the moving jam has emerged in the right lane.

4.7. Extension of free flow recovering and vehicle separation

In traffic flow with identical vehicles, vehicles accelerate to free flow at the downstream front of synchronized flow that is fixed at the bottleneck. In heterogeneous flow with different driver characteristics and/or vehicle parameters, this free flow recovering downstream of the congested bottleneck is accompanied by the vehicle separation effect (section 4.1).

However, in heterogeneous flows this free flow recovering exhibits an additional peculiarity. This peculiarity is the appearance of spatially extended regions of free flow recovering. Downstream of a congested bottleneck regions appear where the average speed is lower than the average speed in free flow. These regions of free flow recovering propagate downstream of the congested bottleneck (figures 10(a), 13(b), (c) and 14). The occurrence of spatially extended regions of free flow recovering can be one of the possible explanations of empirical results where downstream of a congested bottleneck spatially extended regions of lower average speed have been found [53]. In particular, in heterogeneous flow with 50% fast vehicles and 50% slow long vehicles these spatially extended regions of free flow recovering are relatively large (figure 14).

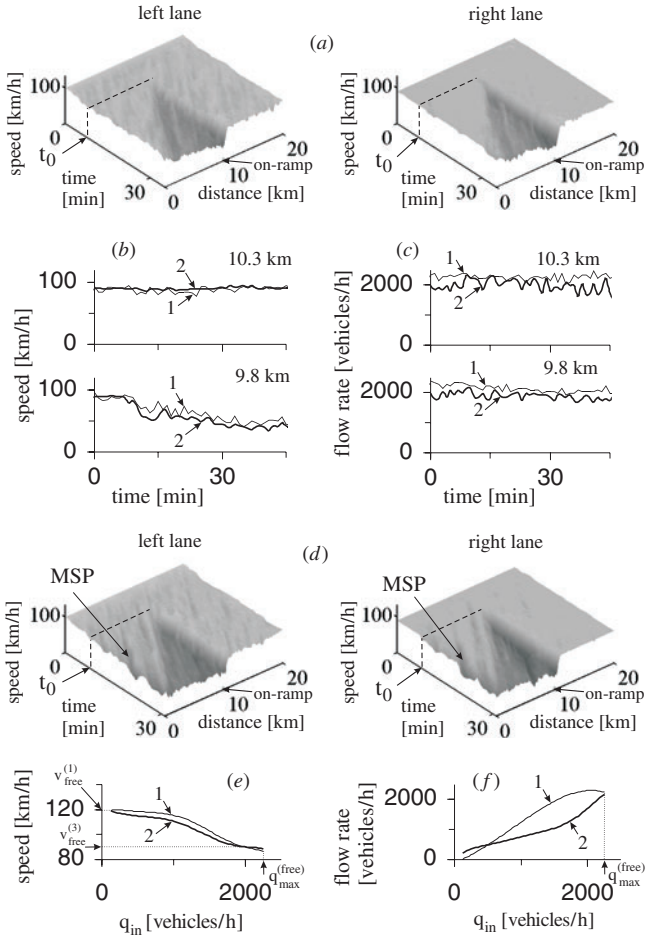

Figure 18. Weak heterogeneous traffic flow: emergence of SPs (*a*)–(*d*) and average vehicle speed and average flow rate in free flow as functions of the incoming flow rate $q_{\rm in}$ (*e*), (*f*). (*a*), (*d*) Speed distributions in time and space in the left and right lanes. (*b*), (*c*) Vehicle speed (*b*) and flow rate (*c*) in the left lane (curves 1) and in the right lane (curves 2) for the WSP at the on-ramp bottleneck shown in (*a*). (*e*), (*f*) One hour average vehicle speed and flow rate in free flow in the left (curves 1) and the right (curves 2) lanes. In (*b*), (*c*) one minute average data of virtual detectors are shown. In (*d*) the arrow shows a MSP that emerges spontaneously away from the bottleneck. The flow rates ($q_{\rm on}$, $q_{\rm in}$) are: (*a*) (300, 2235), (*d*) (300, 2310) vehicles $\rm h^{-1}$. $\eta^{(3)} = 3\%$, $\eta^{(1)} = 97\%$.

The occurrence of the spatially extended regions of free flow recovering can be explained by a blocking effect (figure 17): a long vehicle moving in the left lane with its maximum speed $v_{\rm free}^{(3,{\rm left})}$ forces all upstream moving fast vehicles to move with this speed. Only after the long vehicle has changed to the right lane can fast vehicles accelerate to their maximum speed in free flow $v_{\rm free}^{(1)}$. Positions at which this blocking effect occurs are marked by down arrows in figure 17 ($t = 87$ and 88 min).

5. Large fluctuations effect in weak heterogeneous flow

When the percentage of slow vehicles and/or long vehicles gradually decreases, special features of free and congested traffic in heterogeneous flow considered above *gradually*

disappear. None of these special effects in heterogeneous flows is a threshold effect. At a low enough percentage of slow vehicles and/or long vehicles features of free and congested traffic are the same as those in traffic flow with identical vehicles.

However, when the percentage of slow vehicles and/or long vehicles is low, an additional effect in such a weak heterogeneous traffic flow has been found. This effect is the occurrence of large amplitude fluctuations in free flow. These large fluctuations can lead to a random emergence of MSPs away from bottlenecks when the density in free flow is high enough. In figure 18, in accordance with the diagram of congested patterns, a WSP occurs spontaneously at the on-ramp bottleneck (figures 18(*a*)–(*c*)). However, due to large amplitude fluctuations in free flow another MSP emerges spontaneously away from the bottleneck (labelled 'MSP' in figure 18(*d*)). This MSP propagates in free flow regardless of the WSP at the bottleneck.

The physics of these effects is as follows. When the percentage of long vehicles is high enough, there is separation of fast and long vehicles in free flow (section 4.1). When the percentage of long vehicles decreases, the average space gap between long vehicles in the right lane increases. There is a threshold space gap between long vehicles. If the gap is greater than this threshold gap, then some of fast vehicles change to the right lane, i.e., there is no complete vehicle separation in free flow. A fast vehicle moves in the right lane with its maximum speed before the vehicle approaches a long preceding vehicle. After the fast vehicle has reached this long preceding vehicle, the fast vehicle changes to the left lane to overtake the long vehicle. This lane changing of fast vehicles causes large amplitude fluctuations in free flow. These fluctuations lead to spontaneous MSP emergence when density in free flow is high enough. The same effects occur also in heterogeneous traffic flow with fast and slow vehicles of the same vehicle length.

In addition to the large amplitude fluctuations, at a lower percentage of slow and/or long vehicles another effect in free flow is also realized that is well known in both empirical observations and traffic flow modelling (see references in [57, 58]). At lower total flow rates on the road the flow rate in the right lane exceeds the flow rate in the left lane. If the total flow rate increases, then the flow rate in the left lane increases more rapidly than in the right lane. As a result, at a higher total flow rate the flow rate in the left lane is greater than the flow rate in the right lane (figure 18(*f*)). In the model under consideration, this effect occurs because an increase in the total flow rate leads to a decrease in the mean distance between slow and/or long vehicles in the right lane. Therefore, fast vehicles should more frequently change to the left lane for passing. For this reason, beginning at some density in the right lane the flow rate of fast vehicles, which move in the left lane, increases in a greater degree than the increase in the total flow rate on the road.

6. Characteristics of congested pattern propagation in heterogeneous traffic flow

In this section, we derive some general characteristics of wide moving jams and MSPs propagation in heterogeneous flow that consists of vehicles of K different types moving on a multilane road with M lanes. The percentage of vehicles of type i is $\eta^{(i)}$, where $i = 1, 2, \ldots, K$, and $\sum_{i=1}^{K} \eta^{(i)} = 100\%$.

6.1. Velocity of downstream jam front

In traffic flow with vehicles of one type i, the velocity of the downstream front of a wide moving jam is [14]

$$v_{\mathrm{g}}^{(i)} = -\frac{d^{(i)}}{\tau_{\mathrm{del}}^{(\mathrm{a},i)}(0)}, \tag{51}$$

where $d^{(i)}$ is the vehicle length, $\tau_{\rm del}^{({\rm a},i)}(0)$ is the mean time delay in vehicle acceleration at the downstream front of a wide moving jam. This time delay is related to the speed $v = 0$ within the jam. The velocity $v_{\rm g}^{(i)}$ determines the slope of the line J in the flow–density plane (see explanations of the line J in section 3.1). The line J is marked by the line $J^{(1)}$ in figure 1(c) for fast vehicles, by the line $J^{(2)}$ in figure 1(d) for slow vehicles and by the line $J^{(3)}$ in figure 1(e) for long vehicles.

In heterogeneous traffic flow, during some time intervals the downstream jam front can move with more negative velocity in one of the freeway lanes than in the other lanes. This is because vehicles of different types can be distributed non-uniformly between the lanes (see explanations of examples of wide moving jam propagation in heterogeneous flow in section 4.5). However, this effect is compensated on average by lane changing of vehicles to the lane where the velocity of the downstream jam front is more negative. As a result of this lane changing effect, the downstream front of a wide moving jam moves on the road on average with the same mean velocity $v_{\rm g}$ in all lanes. This conclusion is confirmed by numerical simulations discussed in section 4.5.

In order to find this mean velocity $v_{\rm g}$, let us assume that during a time interval $T_{\rm f}$ the downstream jam front propagates a distance $X_{\rm f}$. The average velocity of the front is

$$\tilde{v}_{\rm g} = -X_{\rm f}/T_{\rm f}. \tag{52}$$

During the time interval $T_{\rm f}$ there are $N^{(i)}$ vehicles of each type i ($i = 1, 2, \ldots, K$) that have accelerated from a standstill within the jam at the downstream jam front. The total number of these vehicles is

$$N = \sum_{i=1}^{K} N^{(i)}. \tag{53}$$

The displacement of the front $X_{\rm f}$ can be expressed in terms of the distances $d^{(i)}$ between vehicles inside the jam:

$$X_{\rm f} = M^{-1} \sum_{i=1}^{K} N^{(i)} d^{(i)}. \tag{54}$$

The time interval $T_{\rm f}$ is equal to the sum of all delay times $\tau_{\rm del}^{({\rm a},i)}(0)$ of all N vehicles that has to be divided by the number of the lanes M:

$$T_{\rm f} = M^{-1} \sum_{i=1}^{K} N^{(i)} \tau_{\rm del}^{({\rm a},i)}(0). \tag{55}$$

Taking into account (54) and (55), $\tilde{v}_{\rm g}$ (52) can be written as follows,

$$\tilde{v}_{\rm g} = -\frac{\sum_{i=1}^{K} \tilde{\eta}^{(i)} d^{(i)}}{\sum_{i=1}^{K} \tilde{\eta}^{(i)} \tau_{\rm del}^{({\rm a},i)}(0)}, \tag{56}$$

where $\tilde{\eta}^{(i)} = (N^{(i)}/N)100\%$. If the time interval $T_{\rm f}$ increases, values $\tilde{\eta}^{(i)}$, $i = 1, \ldots, K$ in (56) tend to the percentages $\eta^{(i)}$, $i = 1, \ldots, K$, respectively, and the velocity $\tilde{v}_{\rm g}$ (56) to the mean velocity $v_{\rm g}$:

$$v_{\rm g} = -\frac{\overline{d}}{\overline{\tau}_{\rm del}^{({\rm a})}(0)}, \tag{57}$$

where $\overline{d}$ and $\overline{\tau}_{\rm del}^{({\rm a})}(0)$ are the mean vehicle length and the mean time delay averaged over all

types of vehicles, respectively:

$$\overline{d} = \sum_{i=1}^{K} \eta^{(i)} d^{(i)}/100, \tag{58}$$

$$\overline{\tau}^{(\mathrm{a})}_{\mathrm{del}}(0) = \sum_{i=1}^{K} \eta^{(i)} \tau^{(\mathrm{a},i)}_{\mathrm{del}}(0)/100. \tag{59}$$

For parameters of heterogeneous flow associated with figure 10 formula (57) yields the velocity $v_{\mathrm{g}} = -14.4$ km h^{-1} whereas the mean velocity v_{g} found in numerical simulations is -14.8 km h^{-1}. In heterogeneous flow consisting of fast and long vehicles (figure 14), the corresponding values are $v_{\mathrm{g}} = -21.2$ km h^{-1} (57) and $v_{\mathrm{g}} = -21.9$ km h^{-1}. The difference between analytical and numerical values of the velocity v_{g} can be explained by moving blanks that occur within wide moving jams in numerical simulations (figures 10 and 14). As a result, the average distance between vehicle fronts within the wide moving jams in numerical simulations is slightly greater than the analytical value $\overline{d}$ (58) used in (57). This effect is more essential in heterogeneous flow of fast and long vehicles in which the moving blanks are usually larger. Note that moving blanks often appear within wide moving jams in empirical observations [56].

6.2. Flow rate in jam outflow

The mean velocity v_{g} of the downstream front of a wide moving jam can be written in the well-known form

$$v_{\mathrm{g}} = -\frac{q^{(i)}_{\mathrm{out}}}{\rho^{(i)}_{\mathrm{max}} - \rho^{(i)}_{\mathrm{min}}}, \tag{60}$$

where $q^{(i)}_{\mathrm{out}}$ is the flow rate of vehicles of type i in the outflow from a wide moving jam when free flow is formed in the jam outflow,

$$\rho^{(i)}_{\mathrm{max}} = \eta^{(i)}/100\overline{d}, \tag{61}$$

$$\rho^{(i)}_{\mathrm{min}} = q^{(i)}_{\mathrm{out}}/v^{(i)}_{\mathrm{max}}, \tag{62}$$

$v^{(i)}_{\mathrm{max}}$ is the average speed of vehicles of type i in heterogeneous free flow in the jam outflow, $v^{(i)}_{\mathrm{max}} \leqslant v^{(i)}_{\mathrm{free}}$, $v^{(i)}_{\mathrm{free}}$ is the speed in free flow with vehicles of type i only. From (57) and (60), (61) we obtain

$$q^{(i)}_{\mathrm{out}} = \frac{1}{\overline{\tau}^{(\mathrm{a})}_{\mathrm{del}}(0)}\left(\frac{\eta^{(i)}}{100} - \frac{\rho^{(i)}_{\mathrm{min}}}{\rho_{\mathrm{max}}}\right), \tag{63}$$

where $\rho_{\mathrm{max}} = 1/\overline{d}$. The flow rate in the jam outflow q_{out} is the sum of the flow rates $q^{(i)}_{\mathrm{out}}$, $i = 1, \ldots, K$ for all K types of vehicles:

$$q_{\mathrm{out}} = \frac{1}{\overline{\tau}^{(\mathrm{a})}_{\mathrm{del}}(0)}\left(1 - \frac{\rho_{\mathrm{min}}}{\rho_{\mathrm{max}}}\right), \tag{64}$$

where $\rho_{\mathrm{min}} = \sum_{i=1}^{K} \rho^{(i)}_{\mathrm{min}}$.

6.3. Velocity of downstream front of MSP

Let us compare velocities of the downstream fronts of a wide moving jam and a MSP in heterogeneous flow. Whereas the velocity v_g (57) of the downstream front of a wide moving jam is a characteristic parameter that does not depend on initial conditions, the velocity of the downstream front of the MSP is *not* a characteristic parameter.

To show this, we use (57) to obtain the mean velocity v_{down} of the downstream front of an MSP in heterogeneous flow. Let us assume that all vehicles within an MSP move with nearly the same vehicle speed v_{syn}. In the system coordinate moving with the velocity v_{syn}, vehicles within the MSP do not move. The average distance between these vehicles is $\overline{\Delta x} = \overline{g} + \overline{d}$, where $\overline{g}$ is the average vehicle space gap within the MSP. The mean velocity v_{down} can be found if in (57) the mean distance $\overline{d}$ and the mean time delay $\overline{\tau}^{(a)}_{del}(0)$ are replaced by $\overline{\Delta x}$ and $\overline{\tau}^{(a)}_{del}(v_{syn})$, respectively. Then in the motionless system coordinate

$$v_{down} = v_{syn} - \frac{\overline{g} + \overline{d}}{\overline{\tau}^{(a)}_{del}(v_{syn})}. \tag{65}$$

Values v_{syn} and $\overline{g}$ can change within an MSP over time and they can also be different for different MSPs. Thus, in accordance with numerical results discussed above the velocity v_{down} (65) is not a characteristic parameter.

7. Discussion

The model we presented reproduces many general empirical features of traffic flow. In particular, different driver behavioural characteristics and different vehicle parameters lead to the well-known lane specific behaviour in free traffic flow: fast vehicles use mostly the left (passing) lane, whereas slow and long vehicles use mostly the right freeway lane. This is the vehicle lane separation effect in free flow. As a result, the average speed in free flow in the left lane is higher than the average speed in the right lane. The vehicle lane separation effect is realized when the percentage of slow and/or long vehicles is compatible with the percentage of fast vehicles. When the percentage of slow and/or long vehicles is low enough, fast vehicles also move in the right lane. In this case, the vehicle lane separation effect does not occur when the flow rate is high enough.

In weak heterogeneous flow in which the percentage of slow and/or long vehicles is low, large amplitude fluctuations can appear in free flow associated with passing of fast vehicles when they approach slow (long) vehicles in the right lane. At high enough flow rate in free flow these large amplitude fluctuations can be comparable with fluctuations at bottlenecks. This can cause an F→S transition away from bottlenecks. This is observed in empirical data [15].

A microscopic traffic flow theory presented in this paper enables us to arrive at the following conclusions about features of the onset of congestion (F→S transition) and congested patterns in heterogeneous traffic flow:

(i) There are some traffic pattern features that are qualitatively the same in traffic flow with identical vehicles and in heterogeneous traffic flows with different driver behavioural characteristics and different vehicle parameters. These *fundamental* pattern features are:
   (a) Types of phase transitions in traffic flow.
   (b) Types of congested patterns at a freeway bottleneck.
   (c) The diagram of the patterns at different traffic demand.

(ii) There are, however, some specific features of congested patterns at freeway bottlenecks in heterogeneous traffic flow:
   (1) The critical amplitude of a local perturbation needed for an F→S transition in the left (passing) lane can be greater than the critical amplitude in the right lane. As a result, there can be a random time delay in MSP emergence in the left lane after the MSP has appeared in the right lane.
   (2) There can be a random time delay in moving jam emergence in the left lane after the moving jam has emerged in the right lane in the pinch region of a GP. During jam propagation in the right lane the moving jam appears also in the left lane.
   (3) If a wide moving jam propagates on a road, there can be some time intervals when the positions of the downstream jam fronts in the left and the right lanes are different. However, there is also an opposite effect of synchronization of these positions. As a result, the downstream jam front propagates on average with the same mean velocity in both lanes. At parameters of the heterogeneous flow chosen for this simulation this characteristic velocity is the same for different wide moving jams.
   (4) There can be a partial destruction of the speed synchronization between different lanes at higher speeds of synchronized flow.
   (5) Downstream of a congested bottleneck spatially extended regions of free flow recovering can appear when vehicles accelerate to free flow at the downstream front of a congested pattern at the bottleneck.

Note that all special pattern properties of item (ii) *gradually disappear* when the differences between driver behavioural characteristics and vehicle parameters in traffic flow decrease. This gradual transformation from heterogeneous traffic flow to traffic flow with identical vehicles does not qualitatively change the fundamental traffic pattern features of item (i).

References

[1] Gartner N, Messer C and Rathi A (ed) 1997 *Revised Monograph on Traffic Flow Theory* (*Spec. Rep.* 165) (Washington, DC: TRB)
[2] Wolf D E 1999 *Physica* A **263** 438
[3] Chowdhury D, Santen L and Schadschneider A 2000 *Phys. Rep.* **329** 199
[4] Helbing D 2001 *Rev. Mod. Phys.* **73** 1067–141
[5] Nagatani T 2002 *Rep. Prog. Phys.* **65** 1331–86
[6] Nagel K, Wagner P and Woesler R 2003 *Oper. Res.* **51** 681–716
[7] Lesort J-B (ed) 1996 *Transportation and Traffic Theory, Proc. 13th Int. Symp. on Transportation and Traffic Theory* (Oxford: Elsevier)
[8] Ceder A (ed) 1999 *Transportation and Traffic Theory, Proc. 14th Int. Symp. on Transportation and Traffic Theory* (Oxford: Elsevier)
[9] Taylor M A P (ed) 2002 *Transportation and Traffic Theory in the 21st Century, Proc. 15th Int. Symp. on Transportation and Traffic Theory* (Amsterdam: Elsevier)
[10] Wolf D E, Schreckenberg M and Bachem A (ed) 1996 *Traffic and Granular Flow* (Singapore: World Scientific)
[11] Schreckenberg M and Wolf D E (ed) 1998 *Traffic and Granular Flow '97, Proc. Int. Workshop on Traffic and Granular Flow* (Singapore: Springer)
[12] Helbing D, Herrmann H J, Schreckenberg M and Wolf D E (ed) 2000 *Traffic and Granular Flow '99, Proc. Int. Workshop on Traffic and Granular Flow* (Heidelberg: Springer)
[13] Fukui M, Sugiyama Y, Schreckenberg M and Wolf D E (ed) 2003 *Traffic and Granular Flow '01, Proc. Int. Workshop on Traffic and Granular Flow* (Heidelberg: Springer)
[14] Kerner B S 1998 *Phys. Rev. Lett.* **81** 3797
[15] Kerner B S 2002 *Phys. Rev.* E **65** 046138
[16] Kerner B S 2002 *Preprint* cond-mat/0211684
Kerner B S 2004 *Physica* A **333** 379–440
[17] Kerner B S 1998 *Proc. 3rd Symp. on Highway Capacity and Level of Service* vol 2 ed R Rysgaard (Denmark: Road Directorate, Ministry of Transport) pp 621–42

[18] Kerner B S 2000 *Trans. Res. Rec.* **1710** 136
[19] Kerner B S 2000 Phase transitions in traffic flow *Traffic and Granular Flow' 99* ed D Helbing, H J Herrmann, M Schreckenberg and D E Wolf (Heidelberg: Springer) pp 253–84
[20] Kerner B S 2001 *Netw. Spatial Econ.* **1** 35
[21] Kerner B S 1999 *Trans. Res. Rec.* **1678** 160–7
[22] Kerner B S and Klenov S L 2002 *J. Phys. A: Math. Gen.* **35** L31
[23] Kerner B S, Klenov S L and Wolf D E 2002 *Preprint* cond-mat/0206370
Kerner B S, Klenov S L and Wolf D E 2002 *J. Phys. A: Math. Gen.* **35** 9971
[24] Kerner B S and Klenov S L 2003 *Phys. Rev.* E **68** 036130
[25] Davis L C 2004 *Phys. Rev.* E **69** 016108
[26] Lee H K, Barlović R, Schreckenberg M and Kim D 2004 Mechanical restriction versus human overreaction triggering congested traffic states *Preprint* cond-mat/0404315
Lee H K, Barlović R, Schreckenberg M and Kim D 2004 *Phys. Rev. Lett.* **92** 238702
[27] Jiang R and Wu Q S 2004 *J. Phys. A: Math. Gen.* **37** 8197–213
[28] Daganzo C F 1999 A behavioral theory of multi-lane traffic flow: part I. Long homogeneous freeway sections *Research Report UCB-ITS-RR-99-5* (Berkeley, CA: University of California)
Daganzo C F 2002 *Trans. Res.* B **36** 131–58
[29] Daganzo C F 2002 A behavioral theory of multi-lane traffic flow: part II. Merges and the onset of congestion *Research Report UCB-ITS-RR-99-6* (Berkeley, CA: University of California)
Daganzo C F 2002 *Trans. Res.* B 159–69
[30] Treiber M and Helbing D 1999 *J. Phys. A: Math. Gen.* **32** L17
[31] Elefteriadou L, Roess R P and McShane W R 1995 *Trans. Res. Rec.* **1484** 80–9
[32] Persaud B, Yagar S and Brownlee R 1998 *Trans. Res. Rec.* **1634** 64–9
[33] Hall F L, Hurdle V F and Banks J H 1992 *Trans. Res. Rec.* **1365** 12–8
[34] *Highway Capacity Manual* 2000 (Washington, DC: TRB)
[35] Banks J H 2002 *Trans. Res. Rec.* **1802** 225–32
[36] Kerner B S 2004 *The Physics of Traffic* (Berlin: Springer)
[37] Barlovic R, Santen L, Schadschneider A and Schreckenberg M 1998 *Eur. Phys. J.* B **5** 793
[38] Knospe W, Santen L, Schadschneider A and Schreckenberg M 2000 *J. Phys. A: Math. Gen.* **33** L477
[39] Takayasu M and Takayasu H 1993 *Fractals* **1** 860
[40] Knospe W, Santen L, Schadschneider A and Schreckenberg M 2002 *Phys. Rev.* E **65** 015101(R)
[41] Krauß S, Wagner P and Gawron C 1997 *Phys. Rev.* E **53** 5597
[42] Gipps P G 1981 *Trans. Res.* B **15** 105–11
[43] Krauß S 1998 *PhD Thesis* DRL-Forschungsbericht 98-08 Köln
[44] Bovy P H L (ed) 1998 *Motorway Analysis: New Methodologies and Recent Empirical Findings* (Delft: Delft University Press)
[45] Neubert L, Santen L, Schadschneider A and Schreckenberg M 1999 *Phys. Rev.* E **60** 6480
[46] Nagel K, Wolf D E, Wagner P and Simon P 1998 *Phys. Rev.* E **58** 1425
[47] Rickert M, Nagel K, Schreckenberg M and Latour A 1996 *Physica* A **231** 534
[48] Knospe W, Santen L, Schadschneider A and Schreckenberg M 1999 *Physica* A **265** 614
[49] Koshi M, Iwasaki M and Ohkura I 1983 *Proc. 8th Int. Symp. on Transportation and Traffic Theory* ed V F Hurdle *et al* (Toronto, Ontario: University of Toronto Press) p 403
[50] Gurusinghe G S, Nakatsuji T, Azuta Y, Ranjitkar P and Tanaboriboon Y 2003 *Preprints of the 82nd TRB Annual Meeting* TRB Paper No 03-4137 (Washington, DC: TRB)
[51] Wagner P and Lubashevsky I 2003 *Preprint* cond-mat/0311192
[52] May A D 1990 *Traffic Flow Fundamentals* (Englewood Cliffs, NJ: Prentice-Hall)
[53] Persaud B and Hurdle V F 1988 *Trans. Res. Rec.* **1194** 191–8
[54] Leutzbach W 1988 *Introduction to the Theory of Traffic Flow* (Berlin: Springer)
[55] Kerner B S and Konhäuser P 1994 *Phys. Rev.* E **50** 54–83
[56] Kerner B S and Rehborn H 1996 *Phys. Rev.* E **53** R1297–300
[57] Brilon W and Wu H 1999 *Traffic and Mobility* ed W Brilon, F Huber, M Schreckenberg and H Wallentowitz (Berlin: Springer) p 163
[58] Wagner P 1995 *Traffic and Granular Flow* ed D E Wolf, M Schreckenberg and A Bachem (Singapore: World Scientific) p 199